CPG-Based Prostheses Control

Master's project in Bioengineering and Biotechnology

Carried out in the
Biomechatronics Laboratory
At the
Massachusetts Institute of Technology
Under the supervision of
Prof. Hugh Herr, PhD

Under the direction of
Prof. Auke Ijspeert, PhD
In the
Biorobotics Laboratory
At the
Swiss Federal Institute of Technology, Lausanne

Marc LOUIS

Department of Life Sciences & Technology

École Polytechnique Fédérale de Lausanne

Lausanne, EPFL 2010

To my loving parents.

Acknowledgements

First and above all I thank God from all my heart. I am deeply thankful to my supervisor, Pr Auke Ijspeert for his support, guidance and enthusiasm about this project. I owe a profound gratitude to Pr Hugh Herr who granted me this unique opportunity and kindly welcomed me within the Biomechatronics group. It is a pleasure to thank, from the bottom of my heart, those who made this project possible Mr O.E., Mrs G.G-L. and Mr R.O. by funding most of it through their foundation. I would like to express my gratitude to Renaud Ronsse, whose encouragement, in depth guidance and support from the initial to the final level enabled me to develop a good understanding of the subject. I am very grateful to Jesse van den Kieboom for his help with the bipedal model. It is not only an honor for me to have worked with Ernesto Martinez who was particularly dedicated, flexible and helpful. It is also an invaluable blessing to have developed such a friendship with a deeply positive and genuinely good personality. By the way, Ernesto, I let you win our 2am ping-pong games on purpose.
I would like to thank all of my colleagues in the Biomechatronics group at particular, Luke for your help with the AAAKP. Bruce, I want to thank you for your infinite wisdom. This is not sarcasm.
I thank my family, Michel, Saneia, Mathieu and Teta. They constantly and steadily made their support available in a number of ways. I love them. I would also like to thank the friends who supported me during this project, in particular: Tamer El Kholy, Seymour De Picciotto and Damiano Genovese. Words can't express how much I owe Jessica for being here. Lastly, I offer my regards to all of those who supported me in any respect during the completion of the project.

Abstract

In this thesis we describe a strategy to control robotic knees and ankles. A dynamical system is used to generate a position trajectory to control a servo motor replacing the missing joint. The dynamical system consists in a pool of coupled oscillators modeling a central pattern generator (CPG).
As a first step, anthropometric trajectories of the knee and ankle are learned by the system through the convergence of the oscillators to the specific frequencies, corresponding amplitudes and phase relations. The same system is then used to play back these trajectories. As a sensory feedback to trigger the playback we use one adaptive frequency oscillator to synchronized with the acceleration from the thigh. We use a bipedal model in a physics-based robot simulation environment to test the proposed system. Finally we present a simple hardware implementation of this system on the Agonist-Antagonist Active Knee prototype.

Contents

List of Figures

Chapter 1

Introduction

"You should go outside, take a walk". That sounds like a good advice to give to someone who needs to rest his mind. This illustrates how little we have to think about placing one leg ahead of the other in order to achieve walking and go forward. Yet, this is a different story for an impaired person such as an amputee. When a human undergoes a lower limb amputation he does not only lose a body part. His integrity and in some cultures, his dignity are diminished as well[1].

Naturally, attempts to restore body parts started very early in History. Prosthetic toes have been found as early as in the ancient Egyptian civilization [4]. Since then, a multitude of different prosthesis designs attempting to restore transtibial and transfemoral amputees mobility have been developed. Their variety reflects the one of amputation configurations, design considerations and approaches. But yet, most of them have one common point: they do not restore the lost muscles net power generation. In that sense they are considered as passive devices.

Indeed, because they do not bring back the ability of net work generation at the impaired legs, passive prostheses are not able to fully restore normal locomotive function during many locomotive activities, including level walking, walking up stairs and along slopes [2, 5, 6]. This is particularly true for transfemoral amputees, who cannot for instance walk upstairs in a step-over-step manner. Regarding transtibial amputees, depending on the general health of the patient, the

[1]Source: Discussion with a prosthetist from the Indian Jaipur Foot organization during the Developing World Prosthesis class at MIT.

biomechanical challenges are more subtle but still of great impact. They involve increased energy expenditure during walking, slower self-selected speed and assymetric gait causing extra strain on the sound joints [7, 8]. A healthy ankle produces the largest burst of torque among all joints during walking. Thus its impairment following amputation causes an increased metabolic energy expenditure by at least 20% [9] (bilateral amputee) as compared to a healthy subject. This extra metabolic energy expenditure is comparable to constantly carrying a 15kg backpack while walking [10].

In the light of these results, a number of companies and research groups focused on the development of active devices capable of providing the amputee with net power from a battery. Section 1.2 of this introduction presents some of these designs. When one develops a power generating device, the question that emerges straight away is the control. One approach that is usually considered is the locomotion model. When following that approach, researchers usually develop models of human locomotion that drive the mechanical design in the first place and the control strategy in the second place. As an example, this is the research avenue used in the Biomechatronics group for the development of an agonist-antagonist active knee [3].

However, understanding how human locomotion is achieved remains one of the great challenges in the filed of neurosciences. The growing field of computational neuroscience intend to provide an understanding of locomotor theories using computational model simulations. In particular, central pattern generators (CPGs) are being modeled and studied extensively giving rise to a synergy between robotics and neuroscience as both field intend to understand, explore, and address the locomotion control problem [11]. CPGs are neural circuits capable of producing neural rhythmic activity. They are found in both vertebrate and invertebrate animals [12, 13]. Several studies have shed light on neuro-locomotor elements of simple animals by modeling CPGs with nonlinear oscillators [14, 15]. These studies not only provided insight of natural neural phenomenon by testing hypothesis on the models but also suggested novel robot control techniques thus contributing to the development of innovative control theories involving CPG models [16]. Also, in terms of bipedal robot locomotion, CPG-based control strategies arouse interest from a number of researchers [17–22]. Moreover, the

use of coupled adaptive oscillators used to model CPGs have recently shown promising results in the field of exoskeleton rehabilitation [23, 24]. Yet, little attention has however been paid to the direct application of a CPG model to a prosthetic control strategy.

1.1 Research Scope and Summary

This being said, most of the works cited above provide promise that a CPG-based control strategy constitute a novel and full of potential research avenue for lower limb prosthetics control. One straightforward argument is that due to its rhythmic character, the walking gait cycle is a good candidate to be controlled by a rhythmic pattern generator. Besides, we will mention that one of the remaining challenges of prosthesis control is speed modulations. Here too, a CPG-based control strategy is an interesting candidate if one exploits the capability of CPGs to synchronize with sensory feedbacks.

In this exploration project, we intend to investigate how a CPG model can be used as a base for the control of a powered knee and ankle prosthesis. For that purpose, we aim to implement a CPG model [1] that is capable of learning the natural knee and ankle positions during the walking gait cycle. We then use the same system to reproduce the learned patterns in a dynamical way. Trajectories played back that way have a similar shape to the natural ones but are generated out of a set of differential equations integrated numerically in real time. Hence they are more suitable to be used as position control for a prosthesis since such a system displays a limit-cycle behavior, which can handle perturbations.

Then we use a physics-based robot simulation software. In that environment we run simulations on a bipedal model in which each joint is modeled by a rotational servo motor. The hips are controlled simply by playing the anthropometric pattern. The ankles and the knees however are controlled with the system described above, with knee and ankle position patterns encoded within. In order to help the CPG play the patterns at the frequency and phase corresponding to the movement of the hips, we implement a sensory-feedback system. The latter takes an acceleration signal from the hip to recognize the phase and frequency of the gait. Its output is then used to trigger the patterns playback. We test

speed modulation by making the hips move at three different speed and observe the quality of the gait tracking by the sensory-feedback system.

Finally, we play the knee trajectory describing two gait cycle from one CPG simulation on the active knee prosthesis developed in the Biomechatronics group using position control.

1.2 Lower Limb Prostheses: State-of-the-Art

Most of us take it for granted, but walking is not as simple as it looks. During a healthy human gait the ankle exerts an important torque to push off the ground. A typical prosthesis does not reproduce the force exerted by a living ankle, resulting in amputees spending much more energy in comparison to walking naturally [7, 8]. In this section we describe some of the state-of-the-art prototypes of prosthetic devices.

1.2.1 Design Consideration

There are a number of elements to consider when designing a lower-limb prosthesis. Manufacturers and researchers often have to make choices about their priorities regarding these factors.

- Storage of the energy acquired through ground contact and using of that stored energy for propulsion. In a number of passive devices this is achieved by material elasticity. Carbon fiber is often used for that purpose.
- Energy absorption: minimizing the effect of high impact on the musculoskeletal system especially at heel strike.
- Ground compliance: stability on uneven terrain and slopes.
- Weight: maximizing comfort, balance and speed.
- Attachment: how the socket will join and fit to the limb.

The last two points are actually of high importance. Somewhat similarly to the development of augmentation exoskeletons, one adds both net power generation

and extra weight. It is then the role of the control to use the power efficiently enough to, at least, compensate the extra weight. For prosthetic devices, one should keep in mind that the weight is situated at the farthest extremity of the limb (in the case of ankle-feet) thus requiring a high torque from the joints above to be ambulated when not actuated. Even if we assume good walking performance, other activities might suffer from the extra weight. Wandering around, walking upstairs and dancing for instance.

Also we will mention that the socket fitting is a crucial element of a satisfying rehabilitation as it determines the amputee confidence in the device. The most ideally controlled device is useless if not well attached to the stump [1]. The amputee has the feeling he might lose the device in any minute, or undergoes pains in the remaining limb every time he steps on it.

1.2.2 Microprocessor Controlled Prosthetic Knees

For trans-femoral amputees, one of the most critical components of the prosthesis is the knee joint. Obviously, a prosthetic knee should provide stability and safety to the patient in order to make him confident in the device and reach a gait kinetics close to the natural one. However this must be achieved with challenging constraints such as weight and cost. The device weight is particularly important as the size of the stump is shorter. Transfemoral amputees are very sensitive to the device's weight as they have to lift it during swing phase to have enough clearance between the toes and the ground. Hence, a heavy prosthesis will increase gait asymmetry and increase stress on the back and the hips. Also, production cost is a major constraint, whether the market spans over a developing country as India, or a developed country such as the USA. In the first case, cost should be low enough for people living with a per capita income of $1,030 USD/year$ [2] to pay for their prosthesis with their own money. In developed countries, insurances usually cover most of the cost generated by the prosthesis. Nevertheless, they sometime refuse to cover expensive devices such as the C-Leg

[1] residual limb

[2] http://www.imf.org

(shown in Fig. 1.1(a)) depending on the patient situation [1]. Moreover, although the physiological advantages of microprocessor controlled knees are proved and numerous, one should also mention that extra cost is not the only drawback. Other practical issues should be taken into account: such devices are usually not waterproof, forcing the amputee to be careful when raining. They also require a battery that has to be charged regularly. That turns the prosthesis into a heavy and awkward to use device in case of battery run out or trouble. Össur Power Knee (Fig. 1.2(a)) for instance, has a battery life of 4 to 5 hours. Also, a device such the Otto Bock C-leg requires that the prosthetist to be approved to calibrate it to the new patient and to perform the maintenance it requires, which is obviously more important than for merely mechanical knees.

Fig. 1.2.2 shows the most popular microprocessor controlled knee prostheses. These prototypes are sometimes called quasi-passive as the stiffness (i.e. damping) at the joint is actively controlled but they do not provide the user net work.

In the Rheo Knee from the Islandic company Össur shown in Fig. 1.1(c) a microprocessor controls the strength of a magnetic field which in turn will determine the viscosity of a magnetorheological fluid thus enabling a controlled resistance of the joint during swing phase. The main advantage of this device is that it can be tuned to be used as a free hinge joint, making some particular activities such as biking easier.

The Otto Bock C-Leg have been one the most successful microprocessor controlled knee prosthesis since it entered the US market in 1999. Like the Rheo Knee, The C-leg does not provide the patient with net work during the gait. However, it allows a variable damping of the prosthetic knee joint via the following mechanism: angular position and velocity as well as forces are measured and are used as input for the algorithm executed by the microprocessor. The latter will then control the opening of small valves that will trigger the amount of hydraulic fluid that can pass into and out of a hydraulic cylinder, thus regulating the extension and compression of a piston connected to the upper section of the

[1] Source: Conversation with Bob Emerson, prosthetist regularly collaborating with the MIT Biomechatronics group, transfemoral amputee himself and C-leg user

(a) **Otto Bock** C-Leg

(b) **Endolite** Smart Adaptive Knee

(c) **Össur** Rheo Knee

(d) **Freedom Innovations** Plié 2.0

Figure 1.1: Commercially available microprocessor controlled knee prosthesis. Pictures from www.ottobock.com - www.endolite.com - www.ossur.com - www.freedom-innovations.com (retrieved August 2010).

knee.

Main advantages [25]:

- Improved stair descent function with C-Leg ($p<.001$).
- Fewer reported stumbles and falls with C-Leg ($p<.05$).

The Smart Adaptive Knee and the Plié 2.0 show behavior similar to the C-leg. However, according to Bob Emerson, they are preferred by smaller number of users.
Fig. 1.2.2 shows a selection of knee prosthesis that intend to provide net work to restore a healthy walking gait.

The Össur Power Knee 1.2(a) is, to the author knowledge, the only powered prosthetic knee commercially available to this day.

The device developed by Sup et. al at Vanderbilt University in Nashvill, TE, USA 1.2(b) [26] is unique in the sense that it is a fully powered robotic leg, including both a knee and an ankle-foot prosthesis.

The AAAKP: [3] In the Biomechatronics group, Cambridge, MA, USA, Hugh Herr, PhD and Ernesto Martinez, PhD candidate are developing a control strategy for the Active Agonist Antagonist Knee prosthesis prototype available in their laboratory.

1.2.3 Prosthetic Ankle-Feet

This section presents some of the state-of-the-art ankle-feet prosthesis. Shown in Fig. 1.3(a), Össur Proprio Foot does not generate net torque. However, it intends to actively adapt the ankle angle depending on the terrain. SPARKy, in Fig. 1.3(b) has an actuator. To the author knowledge, this project is not commercialized neither still under development. The recycling enrgy foot shown in 1.3(c) aims to recycle the energy lost at heel strike in spring to restore it at toe-off. The time release of the spring is microprocessor controlled. The MIT Power-Ankle Foot is actuated by series-spring actuators. The control is achieved

(a) Össur Power Knee

(b) Sup et. al - Vanderbilt Univ. [27]

(c) MIT AAAKP

Figure 1.2: Prototypes of knee prostheses intending to provide the user with net power over the gait cycle.

by a finite state machine [28]. Recent work in the Biomechatronics group shows promising speed modulation results using a reflex-based architecture.

(a) Össur Prorpio Foot

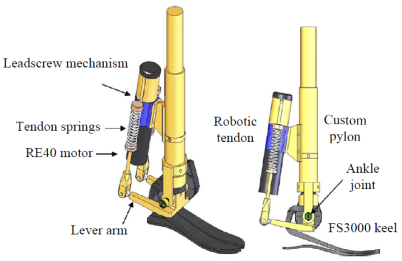

(b) SPARKy - Hitt et. al [29]

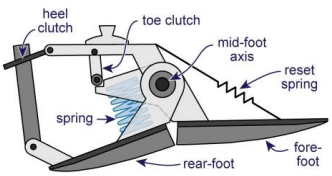

(c) Recycling Foot - S.H. Collins and A.D. Kuo [30]

(d) Power-Ankle Foot - Au et. al [28] and iWalk inc. (Hugh Herr)

Figure 1.3: Prototypes of microprocessor controlled ankle-feet prostheses.

Chapter 2

CPG Model

In this chapter we first describe the nonlinear dynamical system modeling a CPG used to learn and playback joints positions (section 2.1). Secondly, section 2.2 reports the mathematical simulations of the corresponding system for the following two kinds of inputs: a simple signal made of a sum of four sines and the anthropometric ankle and knee trajectoriy for three different walking speeds. The framework described here and used throughout this study is largely inspired by the work of L. Righetti and A. Ijspeert from the Biorobotics Laboratory, EPFL, Lausanne [31].

2.1 Methodology

Section 2.1.1 motivates the choice of the numerical integration method required to simulate the dynamical systems proposed in this study. Then, the construction of a generic CPG model is detailed step by step: first, the equations modeling a basic Hopf oscillator as well as its main features are recalled in subsection 2.1.2. Further, subsection 2.1.3 describes the addition of a general learning rule allowing the oscillators to adapt its intrinsic frequency. Then, we explain the architecture of a set of coupled adaptive frequency oscillators (AFOs) capable of learning any periodic signal in subsection 2.1.4. Finally subsection 2.1.5 describes the two configurations in which the system is actually used to first learn a periodic signal and then play it back.

2.1.1 Numerical Integration

In order to simulate the behavior of the dynamical systems used in this study, one needs to integrate the corresponding ordinary differential equations (ODEs). For that purpose, the forward Euler method is used in both the mathematical simulations (Matlab and Simulink) and the physics-based simulations (Webots). Although it is a first order numerical integration method, it provides an approximation of the solution that is satisfying since the ODEs used in this study are not particularly stiff, i.e. the integration remains numerically stable for the time step used in this study: $0.01s$.

Moreover, as shown in eq. 2.1, which describes the Euler method, it is easy to implement and requires few computational resources. Let us assume we need to numerically integrate the following generic ODE: $\dot{\theta} = F(t, \theta(t))$. Starting from the value of the function to be integrated at the beginning of the integration time t_0 (initial condition), an approximation of the solution is given, step by step by eq. 2.1. This method requires ΔT small enough and an initial condition.

$$\theta(t + \Delta T) = \theta(t) + \Delta T \cdot (F(t, \theta(t)) \tag{2.1}$$

2.1.2 Hopf Oscillator

The building block of the proposed system is the so-called Hopf oscillator [31, 32] defined by equations 2.2 and 2.3 in cartesian coordinates. This system of two non-linear differential equations exhibit a limit cycle behavior: a circle when the two state variables of the system (x, y) are plotted against each other in a phase portrait.

$$\dot{x} = \gamma(\mu - x^2 - y^2)x - \omega y \tag{2.2}$$

$$\dot{y} = \gamma(\mu - x^2 - y^2)y + \omega x \tag{2.3}$$

Where x, y are the system state variables, γ is a constant that modulates the strength of attraction to the limit cycle i.e. the speed with which the trajectory evolves towards the limit cycle. The constant μ is the radius of the limit cycle.

The constant ω represents the angular frequency at which the point $(x(t), y(t))$ rotates around the origin of the limit cycle. Hence, in this basic oscillatory system, there is no way to adapt to any external frequency as the frequency is an intrinsic property of the system.

2.1.3 Adaptive Frequency Oscillators

To develop a system capable of learning an external frequency requires to turn the frequency ω into a state variable of the system. The idea is to assign to this new state variable a general evolution rule to converge to the input frequency. The input $F(t)$ can be seen as a time-dependent force that perturbs the original systems. It has been shown that if the intrinsic frequency $\omega(t_0)$ of the oscillator is close enough to the frequency of $F(t)$, synchronization will occur [33]. This phenomenon is also called entrainment.

$$\dot{x} = \gamma(\mu - r^2)x - \omega(t)y + \epsilon F(t) \tag{2.4}$$

$$\dot{y} = \gamma(\mu - r^2)y + \omega(t)x \tag{2.5}$$

$$\dot{\omega} = -\epsilon F(t)\frac{y}{r} \tag{2.6}$$

This way, the value of $\omega(t)$ will vary throughout the simulation until converging to one of the frequency components of the periodic signal $F(t)$. The largest difference between the intrinsic frequency of the oscillator and the periodic input that still allow entrainment depends directly on the coupling strength (gain of the oscillator). The stronger the gain the larger this difference [31].

2.1.4 Learning System: Generic CPG

For constructing a generic CPG several AFOs have to be coupled in order to learn the different frequency components of the teaching signal. Subsequently, the learned frequencies can be played back to reproduce the learned signal [1, 31]. For this purpose two state variables per single AFO are added to the set of

equations, corresponding to the variables : $\alpha(t)$ and $\phi(t)$. The first one, $\alpha_i(t)$, is the amplitude of the frequency $\omega_i(t)$. The second one, $\phi_i(t)$, is the phase relationship between the oscillator $i \neq 0$ and the oscillator 0.

One advantage of using Hopf oscillators to learn and reproduce signals is that the state variable $x(t)$ is sine-like for small values of coupling gain ϵ. Hence, the output of the system, $Q_{learned}$, is defined as the sum of $x_i(t)$ weighted by the corresponding amplitude $\alpha_i(t)$ (last line 2.8).

Also, by taking as input signal $F(t) = P_{teach} - Q_{learned}$ we have a system that is able to converge to the different frequency components of a periodic signal and to provide the corresponding amplitudes and phase relationships between them. The system can also be interpreted as a dynamic Fourier series representation of the input which will allow to play it back from the same dynamical system with all the advantages that this framework features. The architecture of the whole system is shown in Fig. 2.1. The system of differential equations representing each oscillator i in the network is shown in eq. 2.7.

$$\begin{cases} \dot{x}_i &= \gamma(\mu - r_i^2)x_i - \omega_i y_i + \epsilon F(t) + \tau sin(\frac{\omega_i}{\omega_0}\theta_0 - \theta_i - \phi_i) \\ \dot{y}_i &= \gamma(\mu - r_i^2)y_i + \omega_i x_i \\ \dot{\omega}_i &= -\epsilon F(t)\frac{y_i}{r_i} \\ \dot{\alpha}_i &= \eta x_i F(t) \\ \dot{\phi}_i &= sin(\frac{\omega_i}{\omega_0}\theta_0 - \theta_i - \phi_i) \end{cases} \tag{2.7}$$

$$\begin{aligned} &with, \\ &\quad i = 0, 1, .., N \\ &\quad r_i = \sqrt{x_i^2 + y_i^2} \\ &\quad \theta_i = sign(x_i)cos^{-1}(-\frac{y_i}{r_i}) \\ &\quad F(t) = P_{teach} - Q_{learned} \\ &\quad Q_{learned}(t) = \sum_{i=0}^{i=N} \alpha_i x_i \end{aligned} \tag{2.8}$$

If the input signal to be learned (P_{teach}) is not centered around 0 we add to

the system a simple integrator $\dot{\alpha}_{offset} = \eta F(t)$ in order to learn the offset.

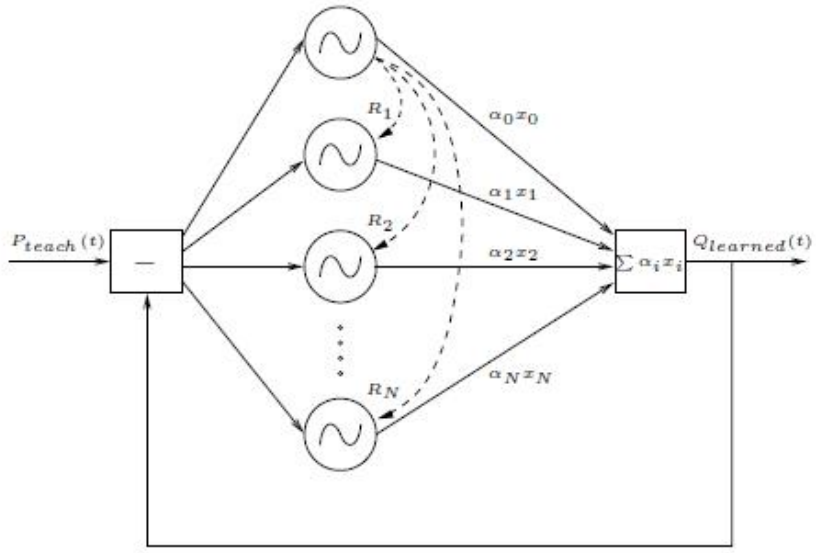

Figure 2.1: Structure of the network of adaptative Hopf oscillators. Refer to [1] for more details.

2.1.5 Playback Systems: Phase Oscillators

The system presented in section 2.1.4 is based on adaptive frequency oscillators and is thus capable of learning a given periodic signal. However, it is also of interest for this study to reproduce (i.e. playback) a learned pattern using a similar system. The playback system presented here is a simplification of the learning system in the sense that it does not contain any of the adaptation mechanisms. Also, to make it simpler the system is written in terms of phase oscillators, that is in polar coordinates, defined by equation 2.9. In the playback case, the oscillator frequencies ω_i are not state variables anymore but constants equal to the parameters learned during the learning step.

$$\begin{aligned}
\dot{\theta}_i(t) &= \omega_i + \tau sin(\frac{\omega_i}{\omega_1}\theta_1(t) - \theta_i(t) - \phi_i), i = 1, .., N. \\
\dot{\theta}_i(t) &= i \cdot \omega_1 + \tau sin(i \cdot \theta_1(t) - \theta_i(t) - \phi_i), i = 1, .., N. \\
\Gamma(t) &= \sum_{i=1}^{N} \alpha_i sin(\theta_i) + \alpha_{offset}.
\end{aligned} \tag{2.9}$$

As the teaching signals we use are periodic, we assume that the frequency components are harmonics, that is $\omega_i = i\omega_0$. In that way the equation can be written in a simpler way as shown in the second line of eq. 2.9.

2.2 Mathematical Simulations

2.2.1 Four Components as Input

This subsection reports the results of an implementation of the programmable CPG described in section 2.1.4. The implementation described here is merely a reproduction of the results described in [1]. This was implemented as a first first step in this project to allow a fair understanding of the system that is used throughout this research.
The system takes a sum of four sine functions each of them having a different frequency ω_i, amplitude α_i and phase ϕ_i $(i = 1, .., 4)$. The simulation is run - the differential equations are numerically integrated - until each oscillator converges to one of the four frequency components composing the input signal P_{teach}:

$$P_{teach} = 0.8sin(15t) + cos(30t) - 1.4sin(45t) - 0.5cos(60t) \tag{2.10}$$

$$= 0.8sin(15t) + sin(30t + \frac{3\pi}{2}) + 1.4sin(45t + \pi) + 0.5sin(60t + \frac{\pi}{2}) \tag{2.11}$$

The parameters and initial conditions are the same as in the aforementioned article (see table 2.2.1). In Fig. 2.2 we observe that after enough simulation time (150s) the learned signal is identical to the teaching signal input as expected. Another interesting observation can be made on the error plot (Fig.2.3), where the absolute value of the error between P_{teach} and $Q_{learned}$ decreases with steps each time an oscillator synchronizes to one of the four frequency components of the teaching signal.

In Fig.2.3 we also observe the state variables ω_i and α_i converging to the values expected which are the frequencies and amplitudes of each of the sines

Parameter	Value
ϵ	0.9
η	0.5
γ	8.0
τ	2

Variable	Initial condition(t_0)
(x_i, y_i)	(1,0) $\forall i = 1..4$
ω_i	$\in [6, 70]$ uniformly
α_i	0.0 $\forall i$
ϕ_i	0.0 $\forall i$

Table 2.1: **Left**: Set of parameters used in eq. 2.7 **for the learning of the four components signal given in eq. 2.10**. **Right**: Initial conditions.

composing P_{teach}.

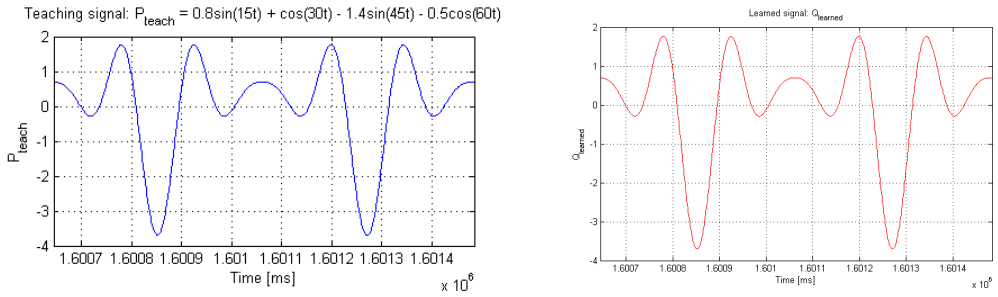

(a) Teaching signal

(b) Learned signal

Figure 2.2: Teaching and learned signal are identical after each oscillator convergence to one of the four frequency components of the teaching signal.

This result is important as it validates the implementation of the programmable CPG when learning a periodic signal replicating the results from [1].

2.2.2 Anthropometric Data Description

The reference signals that are going to be used to actuate the prostheses in this project come from anthropomorphic patterns found in the literature [2]. Like the simple signal investigated above, these periodic signals can also be decomposed in a sum of sine waves, whose amount is unknown a priori.

This section first presents some features of the anthropometric data [2] used throughout this study. Then we explain the calculation to transform the data, normalized with respect to stride percentage, into a continuous and time-dependant signal. The anthropometric trajectories presented here consist of lower limb joint position (flexion/extension): hips, knees and ankles as shown in Fig. 2.4. The

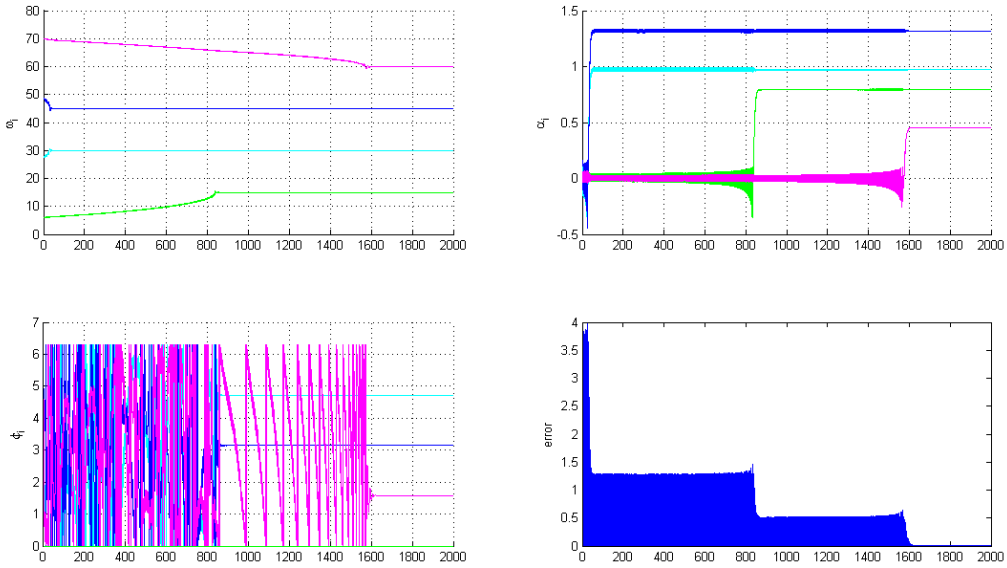

Figure 2.3: Evolution of the state variables of the system when learning the four signal components defined by eq. 2.10. Evolution of the state variables ω_i (top left - rad/s), α_i (top right), ϕ_i (bottom left) and the error between the teaching signal P_{teach} and the learned signal $Q_{learned}$ defined as $abs(P_{teach} - Q_{learned})$. x-axis is simulation time (s).

sign convention used in [2] is shown in Fig. 2.5(a) and Fig. 2.5(b) shows the convention for the bipedal model used in this study, which is presented in more details in section 3.1.1. The data were collected and processed by DA Winter et. al [2].

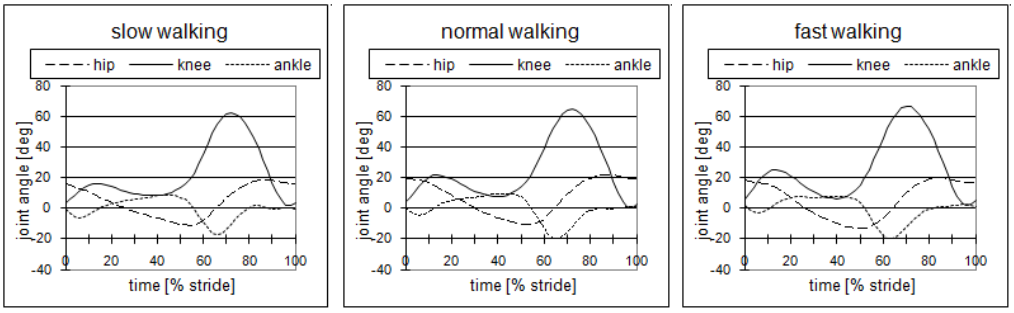

(a) Slow walking (b) Normal walking (c) Fast walking

Figure 2.4: Anthropometric data: joint angles during normal, slow and fast walking (19,19 and 17 subjects respectively.)

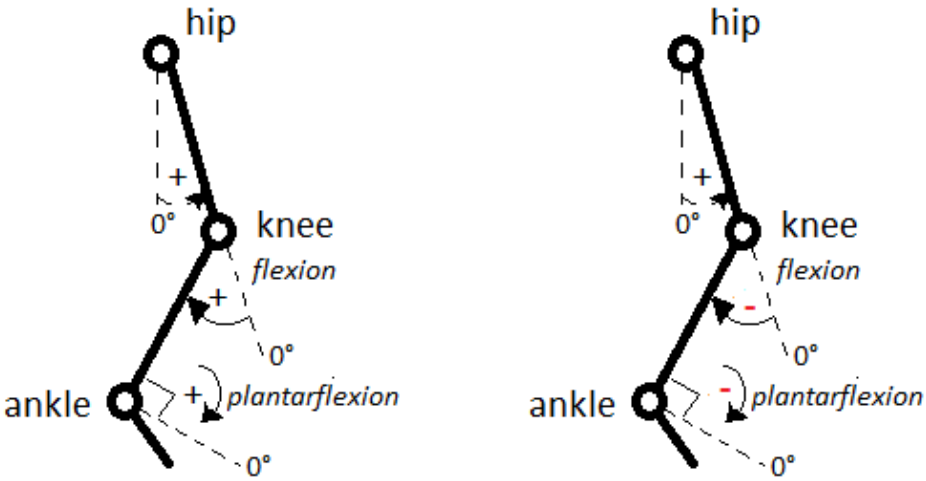

(a) Anthropometric data [2] (b) Webots bipedal model

Figure 2.5: Angles convention used in the anthropometric data from [2] 2.5(a) and in Webots 2.5(b).

The data from [2] being obtained from a number of different subjects, the authors have normalized it as a function of the gait cycle, not time. In order to compute the average time duration of one cycle (stride interval or si), we first compute the first derivative of the positions which gives us the (normalized) angular velocity

$$\hat{v}(t) = v(t) \cdot si$$

As the data available also provides the moment of force τ around each joint and the net power around the joint, we can compute the normalized version of the power p:

$$\hat{p}(t) = \tau(t) \cdot \hat{v}(t)$$

Then we use the least squares method to fit the computed normalized power $\hat{p}(t) = \tau(t) \cdot \hat{v}(t)$ to the power curve provided by the data $p(t) = \tau(t) \cdot v(t)$ to find the value of the stride interval in terms of least squares. The results of this calculation are listed in 2.2. These results seem acceptable as it is commonly accepted that the stride interval of normal walking (self-selected speed) is around 1.2s [1]

Walking speed	Stride interval (s)	Gait freq. (Hz)	Gait freq. (rad/s)
slow	1.55	0.65	4.08
normal	1.30	0.77	4.84
fast	1.14	0.87	5.47

Table 2.2: Computed stride intervals and corresponding gait frequencies.

2.2.3 Anthropometric Ankle and Knee Patterns as Input

Here, the results of the learning system presented in Section 2.1.4 with the anthropomorphic data described above are reported.

The human data used in this study (see section 2.2.2) describe one gait cycle so the input trajectory to be learned is a continuous version of these patterns.

[1] Source: Discussions with Micheal Eilenberg and Jared Markowitz, both PhD candidates in the Biomechatronics laboratory and regularly conducting gait capture experiments. Moreover, [34] reports a stride interval of 1.24s with 0.04 of SD.

Assessment of the number of AFOs to be used: The former section established that a signal made up of four sine waves can be learned with four oscillators. If each has an initial condition close to a frequency component of the signal, each will converge to one of the signal component. However, when learning a signal that has many or an undetermined number of frequency components the question is how many oscillators are required to learn and play back the signal with a satisfying fidelity.

In order to assess the appropriate number of oscillators to generate an output signal close to the input, we tested learning and playback with 3,4,5 and 6 oscillators keeping every other parameter unchanged. It is important to compare the playback pattern and not the learning output as in the latter case the output might be biased (shape closer to the teaching signal because of a high learning gain ϵ). Fig. 2.2.3 shows the comparison between the playback using different numbers of oscillators with the same system.

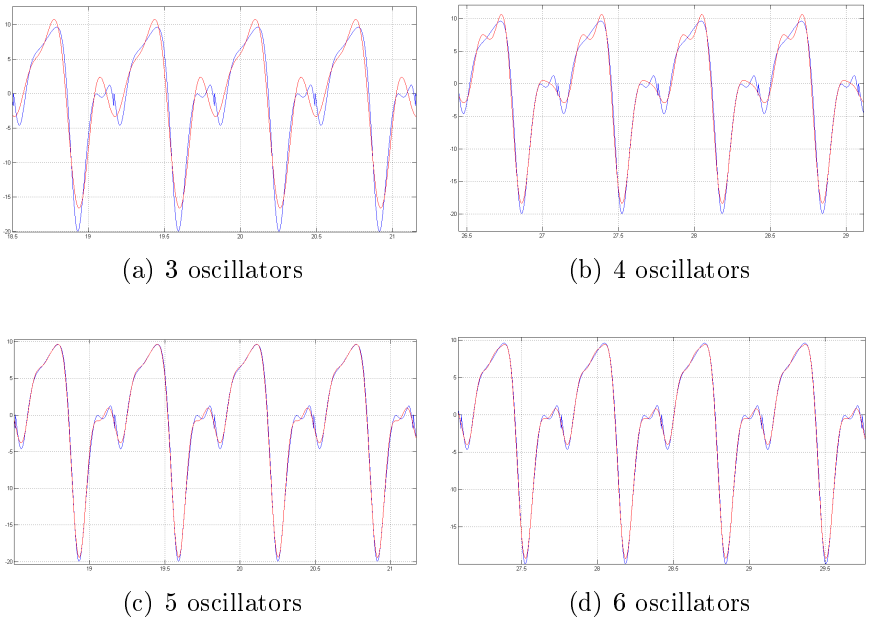

(a) 3 oscillators (b) 4 oscillators

(c) 5 oscillators (d) 6 oscillators

Figure 2.6: Playback with 3,4,5 and 6 oscillators composing the system. Anthropometric ankle pattern (blue) and oscillators playback (red). x-axis: simulation time (s) ; y-axis: ankle angle (deg)

Fig. 2.6(a) and 2.6(b) show the output of the system when it learns the three

Parameter	Value
ϵ	20
η	5
γ	8.0
τ	5
N_{osc}	$3, 4, 5, 6$

Variable	Initial condition(t_0)
x_i	$1.0\ \forall i$
y_i	$0.0\ \forall i$
ω_i	$\frac{1}{n.s.i.} \cdot [1, .., N_{osc}]$
α_i	$0.0\ \forall i$
ϕ_i	$0.0\ \forall i$

Table 2.3: **Left**: Set of parameters used in eq. 2.7 **for the comparison of the output with respect to the number of oscillators**. N_{osc} is the number of oscillators used to learn and to playback. **Right**: Initial conditions. $n.s.i.$ stands for **n**ormal speed **s**tride **i**nterval time in (s).

and four most important frequency components of the ankle pattern (fundamental frequency and two harmonic frequencies). It is visible that the learned pattern is not close enough to the anthropometric pattern. It is interesting to compare Fig. 2.6(c) and 2.6(d) as there is not much improvement by adding a sixth frequency component in the playback signal. Thus, as five oscillators (not including the offset integrator) seem to reproduce the patterns of interest with a good accuracy. This number will be fixed for the rest of this project.

Subsequently, the ankle patterns at the three different walking speeds must be learned by the system.

2.2.4 Learning of the Anthropometric Trajectories

This subsection reports the results of the system in the same configuration as in subsection 2.1.4 for learning the knee trajectory at normal walking speed. All the results of the learning for ankle and knee patterns for all three walking speed are listed in Appendix A.

The parameters defining each pattern are the fundamental frequency, the corresponding amplitudes and phases relationships between the fundamental frequency and the harmonic. These are reported in table 2.

Parameter	Value
ϵ	**20**
η	**10**
γ	8.0
τ	5

Variable	Initial condition(t_0)
(x_i, y_i)	(1.0,0.0) $\forall i = 1..5$
ω_i	$i \cdot f_f$
α_i	0.0 $\forall i$
ϕ_i	0.0 $\forall i$

Table 2.4: **Left**: Set of parameters used in eq. 2.7 **for the learning of the anthropometric knee patter at normal speed**. N_{osc} is the number of oscillators used to learn and to playback. **Right**: Initial conditions. f_f is the fundamental frequency of the pattern.

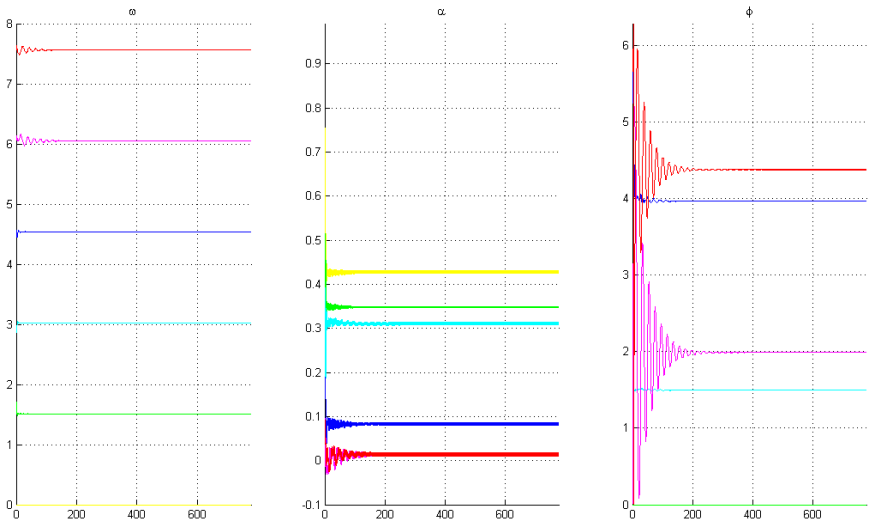

Figure 2.7: Convergence of the state variables ω_i, α_i and ϕ_i (plots left to right) during the learning of the *normal walking speed knee trajectory*. x-axis is learning (i.e. simulation) time in (s). y-axis of the left plot is the frequency in (Hz). Other y-axis are dimensionless.

Oscillator#	1	2	3	4	5
Learned frequencies (rad/s)	9.50	19.01	28.52	38.02	47.53
Corresponding amplitudes (rad)	0.35	0.31	0.08	0.01	0.01
Corresponding phases (dimensionless)	0	1.49	3.96	1.99	4.37

Table 2.5: Learning of the oscillators for *normal* walking speed - *knee* trajectory.

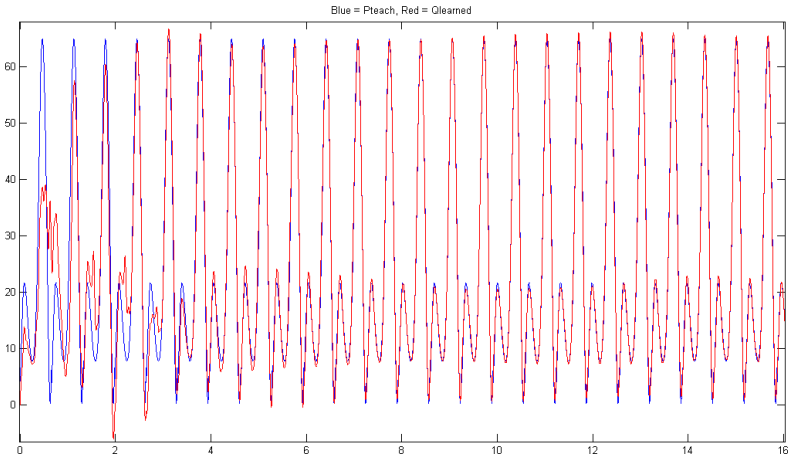

Figure 2.8: First seconds of the learning process for the *normal walking speed knee pattern*. The blue line is the teaching signal i.e. P_{teach} and the red line is the learned signal i.e. $Q_{learned}$. x-axis are simulation time in (s). y-axis are knee angle in (deg).

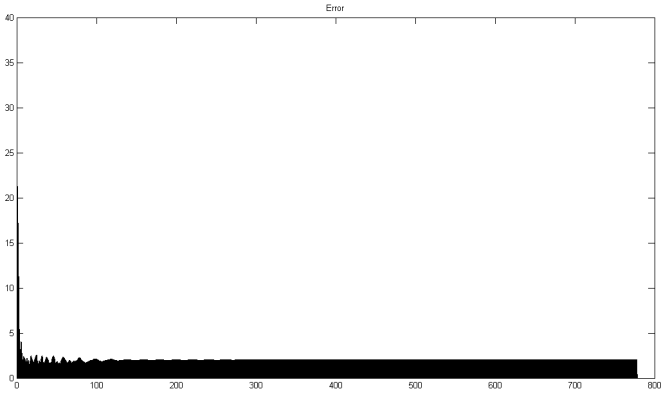

Figure 2.9: Evolution of the error between the teaching signal and the learned signal during the learning of the *normal walking speed knee trajectory*. x-axis is learning (i.e. simulation) time in (s). y-axis is $abs(P_{teach} - Q_{learned})$

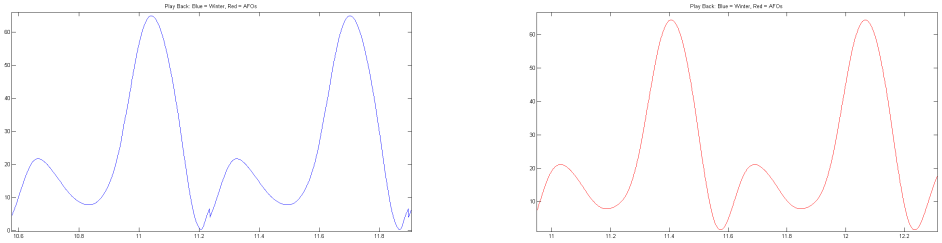

(a) Teaching signal (b) Playback signal

Figure 2.10: Teaching signal (left) and oscillators playback (right) for *normal walking speed knee trajectory*. x-axis are simulation time in (s). y-axis are knee angle in (deg).

Chapter 3

Physics-Based Simulations

In this chapter, we describe the simulation of a bipedal model in Webots, a physics-based robot simulator.

First, in section 3.1, we describe the bipedal model, how it is actuated and what sensory feedback is used. Secondly, section 3.2 describes the results of the bipedal model walking, with simple anthropometric joints trajectory as well as with the CPG-based actuation strategy derived in the previous chapter for knees and ankles. Results of the gait tracking using an AFO as sensory feedback to trigger the CPG-based actuation are also presented in section 3.2. Finally, the results of the physics-based simulations are discussed in section 3.3.

3.1 Methodology

3.1.1 Bipedal Model

The simulations presented in this section were done using a bipedal model simulated in Webots. This model was developed and kindly provided by Jesse van den Kieboom [1], PhD Candidate at the Biorobotics laboratory, EPFL.

As shown in Fig. 3.1 the virtual biped is a model of a nominal male human lower body, accurate in terms of limb length, mass and inertia tensor.

The model consists on a rectangular homogeneous block for the trunk and two legs with four actuated hinge-like DOFs modeling each joint: hip, knee,

[1] jesse.vandenkieboom@epfl.ch

ankle and toe. Each DOF can be controlled given position, torque or velocity. In this work however, we only use position control in order to actuate the hips, knees and ankles. Toes are passive in the sense that their dynamic is modeled by a spring-damper system.

The architecture of the model is purposely kept simple. Indeed, as this study intends to investigate the use of a CPG model to generate joint trajectories using simple sensory feedback, the model does not include any muscle dynamic such as muscle synergies, reflexes or energy storage properties provided by tendons. Also there is no balance control in that model. So in order to prevent falling down during walking this model is supported by a roller cage constraining some of the degrees of freedom of the modeled robot.

This 'security device' causes some unwanted interaction artifacts between the robot and the cage. This decreases the accuracy of the model to a level that is nevertheless still acceptable for the pilot investigations conducted in this thesis.

As a first step, the aim is to control the DOFs of the hip, knee and ankle to follow the anthropometric positions. This way we have a model to assess the performance of a CPG-based controller.

The servo motors used in this model are a simulation of real rotational servo motors and are implemented as predefined nodes in Webots. In this study we use them in the position control using standard proportional feedback with gain P. This P-controller also requires an upper bound for the provided torque. The maximum velocity is also a parameter of the servos. Table 3.1 summarizes the values for the maximum torque available, the maximum velocity and the servo P-gain for each actuated DOF. The P-gain has a default value of 10 which we did not change in this study as the details of the electromechanics are not meant to be investigated. The maximum velocity is chosen large enough not to hinder the joints movements. Similarly the maximum torques are chosen to be large enough to allow the bipedal to go forward. In Fig. 3.2 shows a scheme of the implementation of servos in Webots, displaying only the functions that we use in this work, namely *servo set postion* as well as the fixed parameters listed in table 3.1

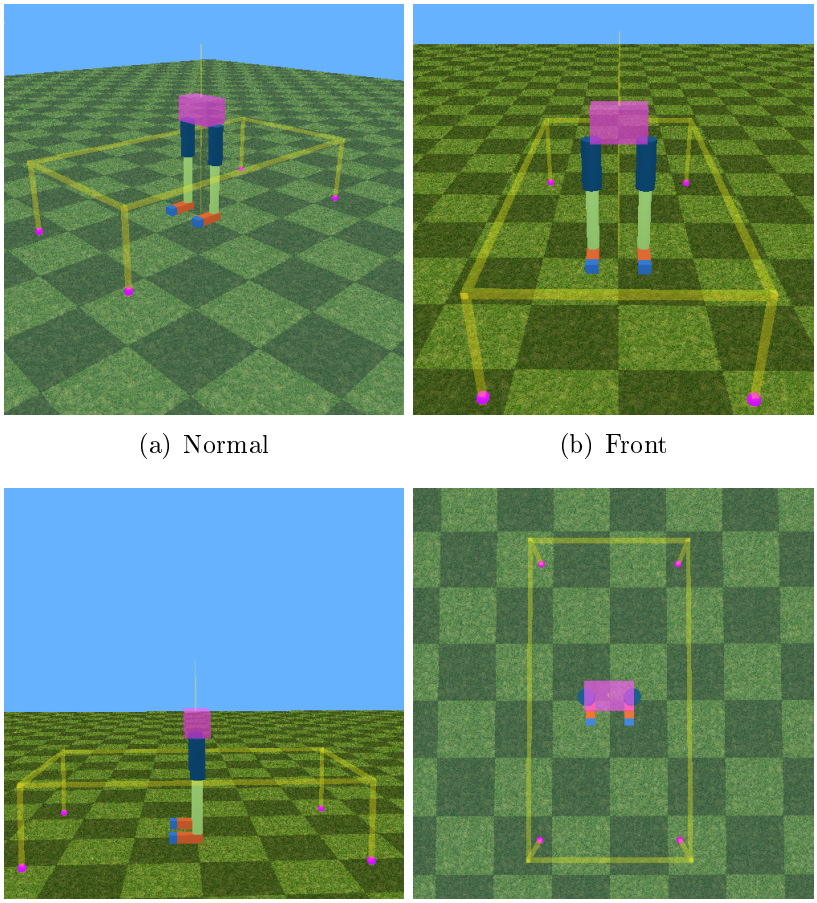

(a) Normal (b) Front

(c) Side (d) Top

Figure 3.1: Views of the bipedal model with eight DOFs and roller cage in Webots.

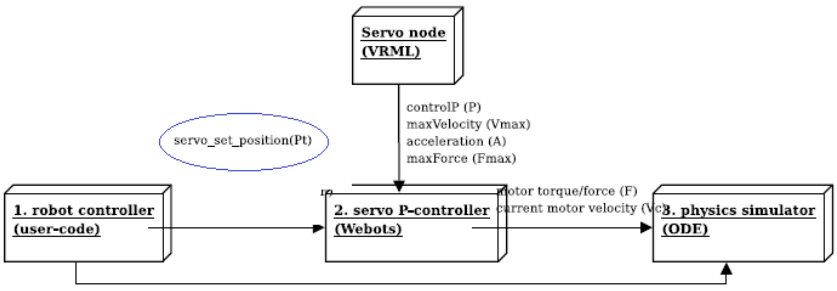

Figure 3.2: Servo control in Webots. Source: Webots Reference Manual release 6.2.4 page 106.

DOF	max torque ($N \cdot m$)	max velocity (rad/s)	P-gain
Hips	500	50	10
Knees	500	50	10
Ankles	500	15	10

Table 3.1: Important parameters of the servos model in Webots.

3.1.2 Sensory Feedback

This subsection focus on the sensory feedback that will be used to control the final prototype presented in this study. We explain how the gait tracking is achieved using this sensory feedback and the pool of playback oscillators. In Fig. 3.3 we show an overview of the proposed system including the gait tracking subsystem constituting the sensory feedback.

3.1.2.1 Acceleration measurements

Among the sensors available in Webots, the gyroscope and the accelerometer seemed to be the most relevant choices to get a signal encoding the gait periodicity. The touch sensor, also available in Webots, was considered but would provide a binary information that would likely decrease the quality of the tracking during varying walking speed.

The accelerometer node provided by Webots models an accelerometer device such as those commonly found in mobile electronics, robots and games devices [1]. It returns acceleration values in a three dimension vector expressed in m/s^2 and simulates the noise usually found on such devices [2]. The accelerometer provides the acceleration along each of the three axis x-y-z in the coordinate system of the accelerometer node, relative to its parent node (the hip servo node).

The gait features we intend to extract out of the acceleration signal are the fundamental frequency and the phase. These variables will then be used as input to a pool of playback oscillators in order to play the patterns at both knees and ankles. Therefore, the phasing of the acceleration within the gait cycle must be determined. In this study the extraction of the instantaneous gait frequency and

[1] Webots Reference Manual, release 6.2.4.
[2] Conversation with Jesse van den Kieboom.

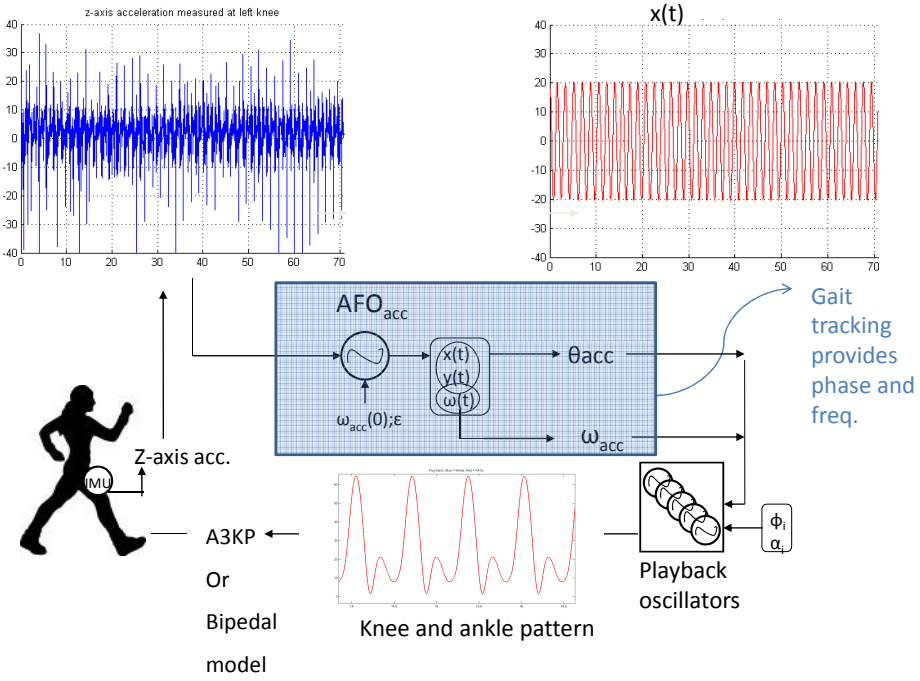

Figure 3.3: Block diagram of the overall system with the gait tracking subsystem in the blue box. IMU stands for Inertia Measurement Unit, a device containing accelerometer and gyroscope providing the input for the gait tracking AFO. A3KP stands for Agonist-Antagonist Active Knee presented in chapter 4.1.

phase is done by the synchronization of one AFO with the acceleration signal. We found that the acceleration signal providing the cleanest periodic pattern is from the z-axis (intersection between sagittal and transverse plane when at rest). Hence, from the rest of this report, the term *acceleration* will refer to *z-axis acceleration* unless specified.

The placement of the accelerometer on the hip: In the conducted simulations the best results are obtained when the acceleration is measured on the thigh. It is likely because the movements on that segment have a more stable pace since the hips servos play the anthropometric pattern regardless of the knees and ankle positions. Therefore the accelerometers on the hip measure a clean motion which is equal to the anthropomorphic data.

3.1.2.2 Gait tracking using one AFO

In section 2.1.4, we presented how coupled oscillators within a negative feedback loop can learn a specific periodic pattern. This was based on a generic learning rule for the state variable ω_i of each oscillator (section 2.6, equation 2.6). Similarly we would like to take advantage of the adaptive frequency feature of the oscillators presented in this study in order to track the frequency and phase of the gait from the acceleration signal. The acceleration signal is used as input of an AFO that synchronizes with it thus extracts the gait frequency and phase. These variables are then used to trigger the pool of AFOs after learning. The equations modeling this gait tracking AFO are shown in 3.1-3.4.

$$\dot{x}_{acc} = \gamma(\mu - r_{acc}^2)x_{acc} - \omega_{acc}y_{acc} + \epsilon_{acc}a_z \tag{3.1}$$

$$\dot{y}_{acc} = \gamma(\mu - r_{acc}^2)y_{acc} + \omega_{acc}x_{acc} \tag{3.2}$$

$$\dot{w}_{acc} = -\epsilon_{acc}a_z(-\frac{y_{acc}}{r_{acc}}) \tag{3.3}$$

$$\dot{\theta}_{acc} = sign(x_{acc})(-acos(-\frac{y_{acc}}{r_{acc}})) \tag{3.4}$$

These equations are a simplified version of the CPG model presented in chapter 2. The parameteres γ and μ are kept the same. The signal that this AFO intend to track, a_z is the output of the z-axis acceleration from the thigh. It replaces $F(t)$ in the CPG model equations. Important parameters of this system are the gain ϵ_{acc} and the initial condition on ω_{acc}. The former is chosen by trial and error and the latter is chosen to match the normal walking speed. Also, depending on the parameters chosen, we observe that ω_{acc} can sometimes lose its synchronization and converge to zero. In order to overcome that problem, a resetting is implemented. This is achieved by putting two conditions on ω_{acc}: if it is close to zero AND the acceleration is not equal to zero (i.e. the subject wants to walk) then ω_{acc} is reset to its initial condition.

Subsequently, the gait variables ω_{acc} and θ_{acc} are used to trigger the frequency and phase of the playback oscillators as shown in eq. 3.5. The constant δ is a fixed phase shift that is manually chosen to match the dynamic obtained from x_{acc} with the desired joint position.

$$\begin{aligned} \dot{\theta}_i(t) &= i \cdot \omega_{acc} + \tau sin(i \cdot \theta_{acc}(t) - \theta_i(t) - \phi_i), i = 1, .., N. \\ \Gamma(t) &= \sum_{i=1}^{N} \alpha_i sin(\theta_i + i \cdot \omega_{acc} \cdot \delta) + \alpha_{offset}. \end{aligned} \tag{3.5}$$

3.2 Results

3.2.1 Walking with the Anthropometric Trajectories

In order to validate the bipedal model, we first feed the servo motors at the hips, knees and ankles with the anthropometric trajectories from [2] at normal speed. The positions of the knees and the ankles are multiplied by -1 in order to be coherent with the angle convention of the bipedal model as explained in Fig. 2.5. As the data describe a gait cycle starting from heel strike [1] we just play it as it is for one leg and half cycle lagged for the other.
The result of this simulation is qualitatively very close to a human gait though it is slightly more jerky. Fig. 3.4 shows a set of snapshots of the bipedal model over

[1] In the literature, heel strike is commonly accepted as a convention for the starting point of a gait cycle.

approximately one gait cycle. In videos 1# and #2 we observe that each heel strike is more of like collision between the foot and the ground than a smooth weight transfer. This is most probably due to the rigid nature of the model that obviously does not take into account any of the human tissue properties (soft tissues and cartilages tendons; or energy storage). All these act to make the interaction of the human with the ground gentler than displayed by the model. Fig. 3.5 shows the result of the actual measured positions of the joints compared to the anthropometric positions commanded to the P-controller. As expected there is a delay between the desired trajectory and the actual position as the amount of torque available and the maximum velocity of the servo motors are limited. Since the delay does not vary much throughout the gait cycle (between $0.05s$ and $0.1s$) it does not affect the quality of the gait.

The hip trajectory is the one tracked with most fidelity as it displays the smallest variations. The knee pattern is also tracked with a satisfying fidelity though neither the anthropometric full extension nor flexion are reached. The ankle pattern is tracked with slightly less fidelity. However its important features are preserved: small plantarflexion at heel strike, dorsiflexion during early stance to go forward and plantarfexion during swing to have enough clearance between the toes and the ground.

Link for the videos that shows the bipedal walking in the configuration described in section 3.2.1: video #1 (normal view) and video#2 (side view).

3.2.2 Walking with the CPG Position Control

In this section we report the results of the bipedal model walking using both the CPG-based playback dynamical system (eq. 2.7), and the thigh accelerometers to specify the fundamental frequency and phase of the main oscillator. Four independent pools of oscillators were used, for both ankles and both knees. The hips servos however play the anthropometric trajectories as in section 3.2.1. In Webots we implemented one gait tracking system per leg. That means one accelerometer at each hip synchronizes to one gait tracking AFO that triggers the

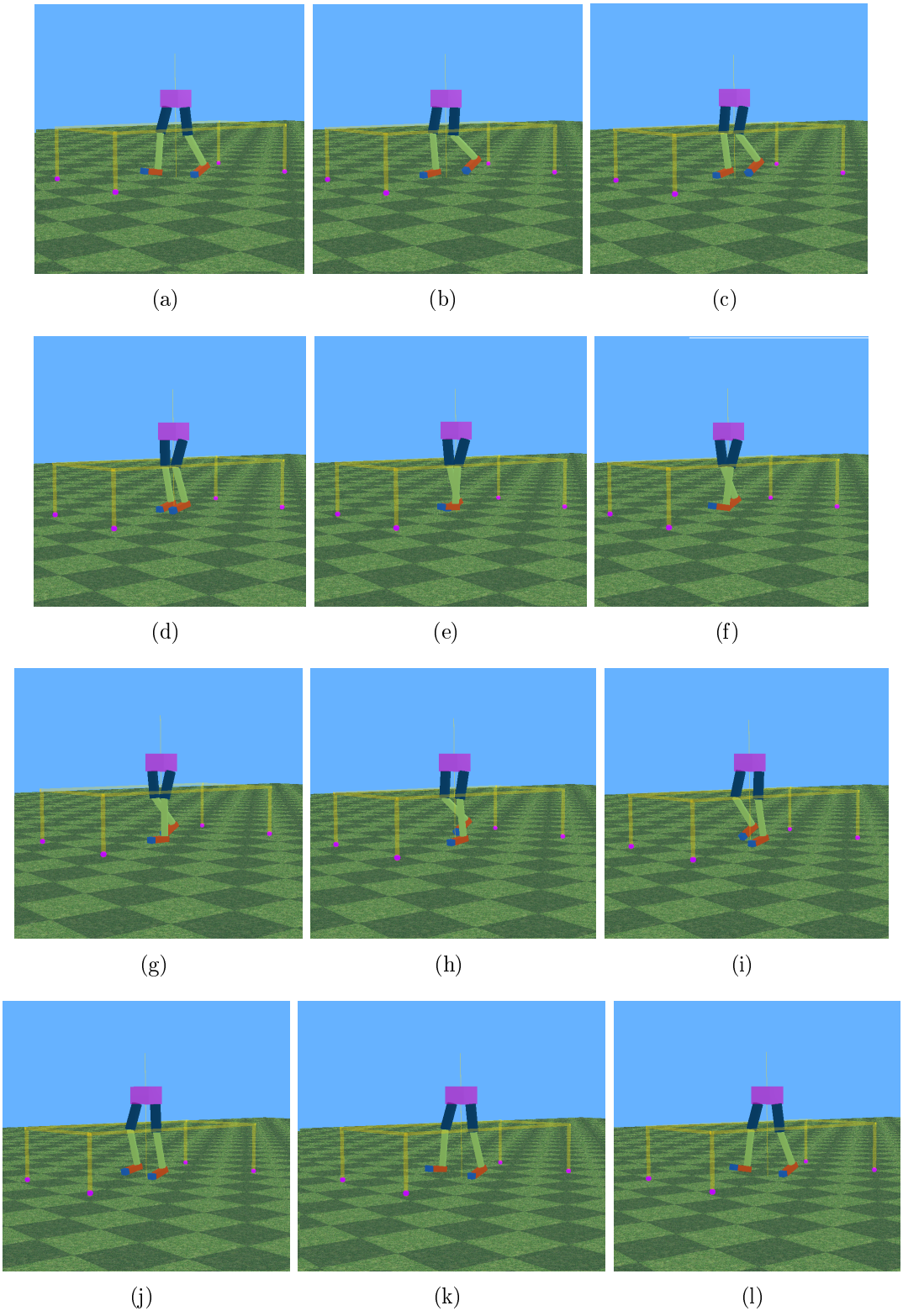

Figure 3.4: Snapshots of one gait cycle of the bipedal model simulation in Webots.

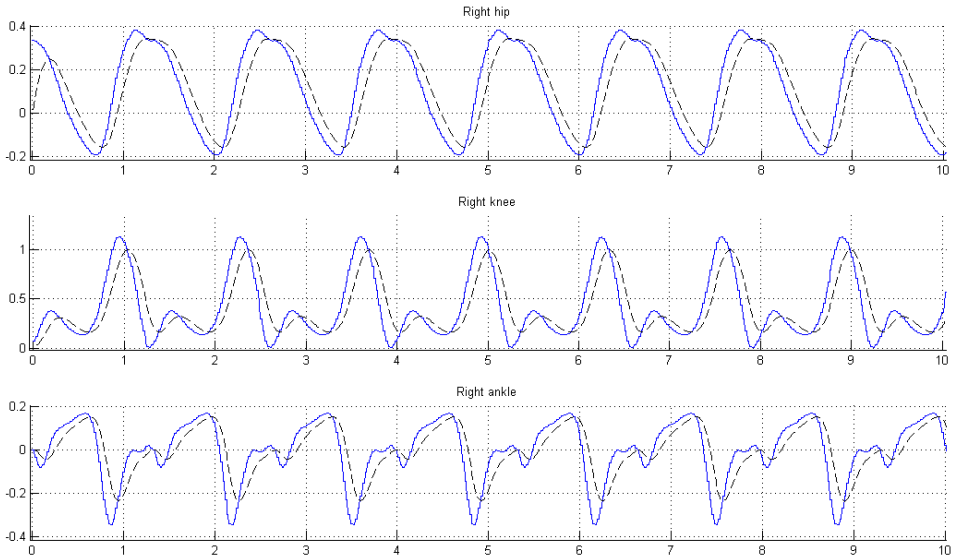

Figure 3.5: Trajectories of right hip, knee and ankle of the bipedal model when walking at normal speed unsing the anthropometric data as input of the controller. Measured positions in dashed black and anthropometric commanded positions in solid blue. x-axis is simulation time (s). y-axis is joint positions according to the anthropometric data convention (see 2.5) (rad)

frequency and phase of the knee and ankle dynamical system pattern playback for each leg as explained in section 3.1.2.2.

In order to test the robustness of the gait tracking system, we implemented a simulation in which the hips start by playing the anthropometric pattern at slow walking speed ($t = 0s$), then abruptly switches to fast walking speed ($t = 30s$) and finally slow down from fast to normal walking speed ($t = 60s$). Section 3.2.2.1 reports the results of the gait tracking system state variables x_{acc} and ω_{acc}. Section 3.2.2.2 shows the results of the trajectories of the three joints. The gain of the gait tracking AFO is $\epsilon_{acc} = 0.7$ and the initial condition on the frequency is $\omega_{acc} = 3.5$.

3.2.2.1 Gait Tracking

In Fig. 3.6 we observe that it takes 10 seconds for the system to stabilize. Then the transition to fast is handled in approximately 10 seconds whereas the transition from fast to normal is done in 5 seconds.

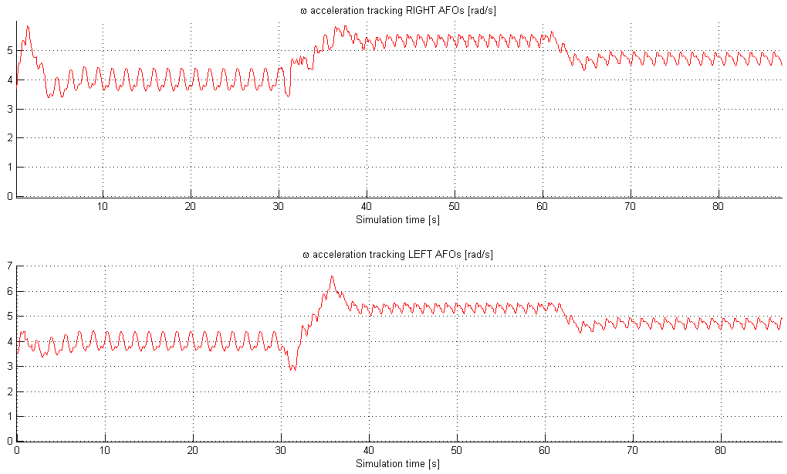

Figure 3.6: Evolution of the state variable ω_{acc} of each gait tracking AFO (rad/s) in red.

3.2.2.2 CPG trajectories playback

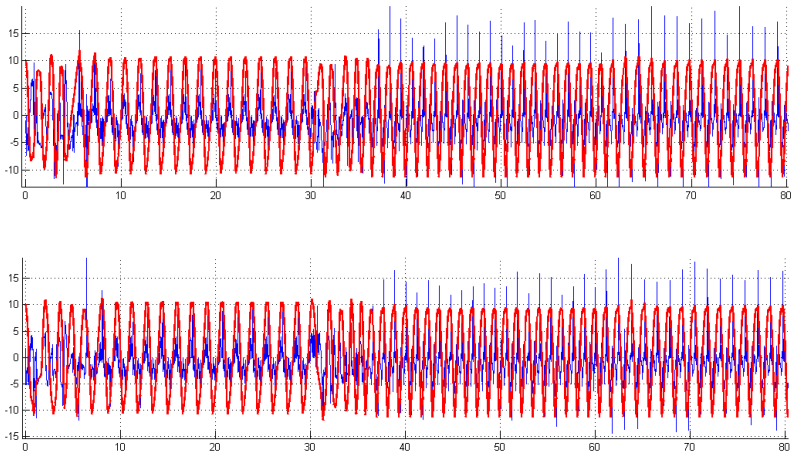

Figure 3.7: Synchronization of the gait tracking AFO during a 90s simulation. z-axis acceleration (m/s^2) in blue. State variable $x_{acc}(t)$ is in red. (dimensionless, not in scale).

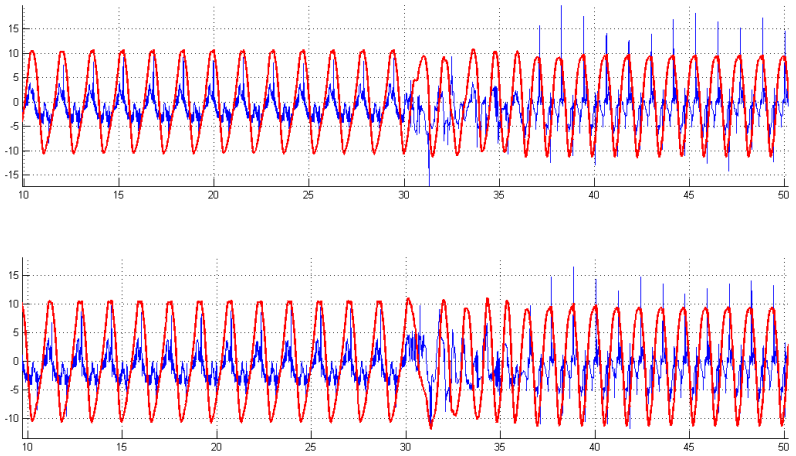

Figure 3.8: Synchronization of the gait tracking AFO from $t = 10s$ to $t = 50s$ of the same simulation. z-axis acceleration (m/s^2) in blue. State variable $x_{acc}(t)$ is in red. (dimensionless, not in scale).

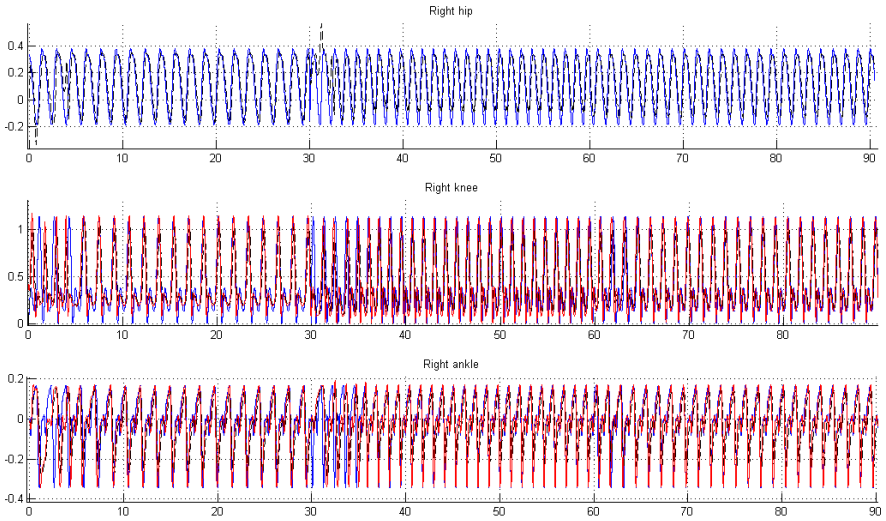

Figure 3.9: Overall simulation. From top to bottom: trajectories of right hip, knee and ankle (rad). Blue is the anthropometric trajectory as reference. Red is the CPG playback. Dashed black is the measured position.

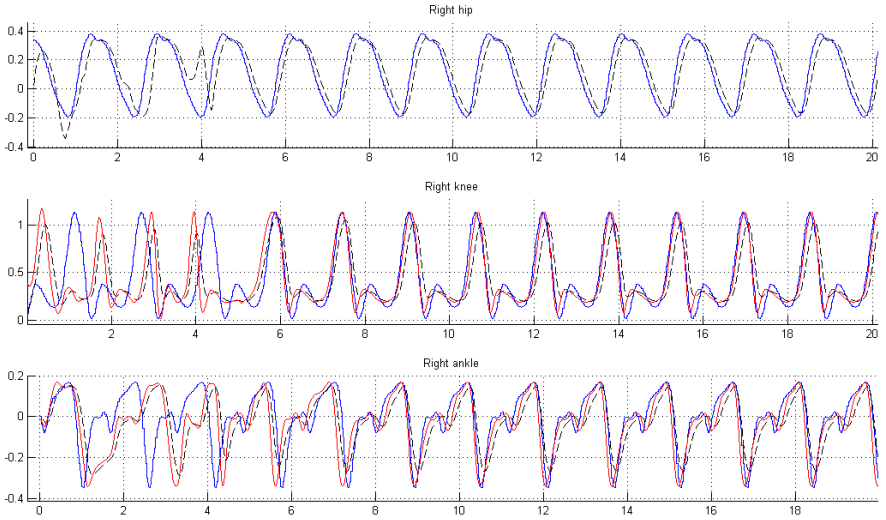

Figure 3.10: First 20 seconds of the simulation: slow walking speed. From top to bottom: trajectories of right hip, knee and ankle (rad). Blue is the anthropometric trajectory as reference. Red is the CPG playback. Dashed black is the measured position.

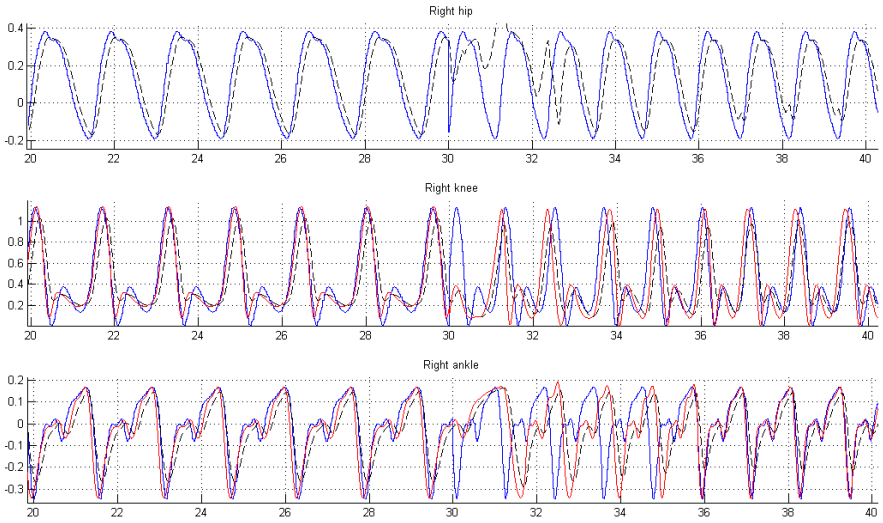

Figure 3.11: Transition from slow to normal. From top to bottom: trajectories of right hip, knee and ankle (rad). Blue is the anthropometric trajectory as reference. Red is the CPG playback. Dashed black is the measured position.

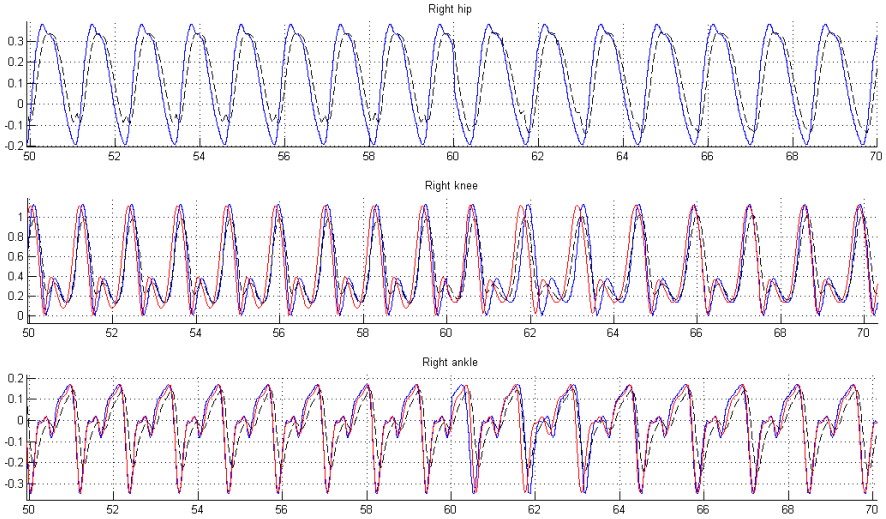

Figure 3.12: Transition from fast walking to normal. From top to bottom: trajectories of right hip, knee and ankle (rad). Blue is the anthropometric trajectory as reference. Red is the CPG playback. Dashed black is the measured position.

Corresponding videos

Link for the videos that shows the bipedal walking in the configuration described in section 3.2.2:
video #3 (10 first seconds)
video #4 (slow to fast walking speed transition)
video #5 (fast to normal walking speed transition)

3.3 Discussion

In this chapter we presented the bipedal model, the gait tracking system and the results of the bipedal walking first playing the anthropometric positions at all joints and second with CPG-actuated knees and ankles using acceleration as sensory-feedback.

3.3.1 Walking with the anthropometric trajectories

A very close to human walking gait is achieved simply by feeding the servos with anthropometric values. The measured trajectories are very satisfying for the hip in particular. Regarding the knee and the ankle, some features of the pattern are lost, and extrema are not reached. However that does not seem to prevent the bipedal model to achieve walking. This being said, one should keep in mind that such a gait requires that the rotational servo motors are able to deliver approximately ten times the estimated human torque. This is probably because a too large p-gain. Another reason for that is probably because of the stiffness of the control especially during stance where the p-controller tries to impose desired positions that are not in phase with the kinetics of the bipedal model while walking. Also, the bipedal model itself might have some inaccuracies regarding the weights of the limbs. We also mention the roller cage might be a cause of increased torque requirement as it absorbs energy in springs to maintain the bipedal model in the appropriate position.

3.3.2 Gait tracking

The results of the gait tracking are very satisfying. The challenge that is overcome here is the stabilization of a closed-loop system, especially at the starting of the gait. This is made possible in part because of the placement of the accelerometers on the hip that move regardless of the movements at the knee or ankle. The transition from slow to fast is achieved but takes approximately 10 seconds in which an unstable gait is involved. That is more than enough to make an amputee stumble and fall. However, one should keep in mind that the speed transition display by the hips motion is an abrupt switch that cannot happen with human, especially carefully walking amputees. Moreover, due to the way it is implemented, the frequency transition implies an abrupt phase shift in the hips movement, which makes the gait tracking task even more challenging for the tracking AFO. The quality of the transition from fast to normal is more remarkable. It is achieved without ω_{acc} resetting or even an unstable gait. The AFO just adapts to the speed decrease in a smooth and stable way within less than 4 seconds. We will recall that this is achieved using only one simple AFO, without filtering the acceleration signal.

3.3.3 CPG position control

The plots showing the trajectories, revealed a distortion of the output of the playback CPG. This is likely the effect of the gait phase θ_{acc} as it is computed from $(x, y)_{acc}(t)$. When using one AFO to synchronize with a signal having a lot of harmonics, like the acceleration used here, the gain ϵ_{acc} of the AFO must be carefully tuned. If too small, no synchronization will occur; if too large, the pattern of the state variables x and y will not look like a simple sine wave. For the value we picked up, namely $\epsilon_{acc} = 0.7$ there is still some bumps appearing on the trajectory of $(x, y)_{acc}(t)$ as shown in Fig. 3.7. We believe that they caused the small distortions in the playback patterns. However, as seen on the movies, an acceptable gait is achieved.

Chapter 4

Hardware Testing on the AAAKP

4.1 Agonist-Antagonist Active Knee Prosthesis Description

This section presents the prosthetic knee device available in the Biomechatronics group: the Agonist-Antagonist Active Knee Prosthesis (AAAKP). It was developed mainly by Ernesto C. Martinez-Villalpando PhD candidate and Hugh Herr PhD, within the Biomechatronics group [1].

First, the design considerations and the model that motivated the design are briefly explained. Then the main characteristics of the design are presented. This includes the overall mechanical architecture, the electromechanics and sensors. For further details about the model optimization, control design architecture and corresponding results the reader is invited to refer to [3]. Most of the explanations and all of the plots in this section are either inspired or reproduced from [3] and from direct discussion with one of the author, Ernesto Martinez-Villalpando.

4.1.1 Assumptions, Hypothesis and Knee Model

The knee prosthesis design presented here derives from the prosthetic knee model [35] shown on the right of Fig. 4.1. The model comprises a variable damper and two series-elastic clutch units to span the knee joint in an agonist-antagonist manner.

[1] MIT Media Laboratory, Cambridge, MA, USA.

It is biomimetic and reproduces human-like knee mechanics when controlled by a variable-impedance control design.

The parameters of the model are the two spring constants (k_E, k_F) that determines the extension and flexion spring stiffness, and the knee flexion and extension angles at which the extension and flexion springs are engaged. The result of the optimization to fit anthropometric torque provided the basis for the controller proposed in [3].

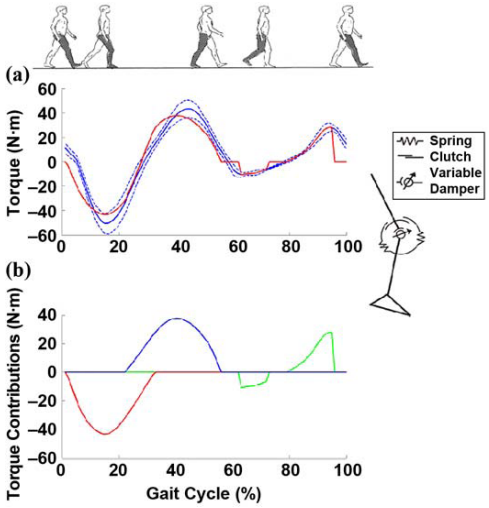

Figure 4.1: Variable-impedance prosthetic knee model. Scheme of the model shown on the right comprises two series-elastic clutches and one variable-damping element. **(a)** Net torque output by the model (red) compared to sound human knee joint (1 subject, 10 trials, self-selected speed = 1.31 m/s, mean is solid blue line and ±SD is dashed blue line). **(b)** Torque contribution from extension (red) and flexion (blue) springs of series-elastic clutch elements as well as variable damping (green). Image copied and text inspired from [3].

4.1.2 The AAAKP Prosthesis Design

Based on the model described above, the AAAKP was built with two series-elastic actuators as shown in Fig. 4.2. Each motor can act independently to engage/disengage the flexion and extension springs by holding or releasing them. However, for the study presented in this report, we use a position control encoder

that commands input current given to both DC motors in order to allow a direct position, i.e. knee flexion angle, control.

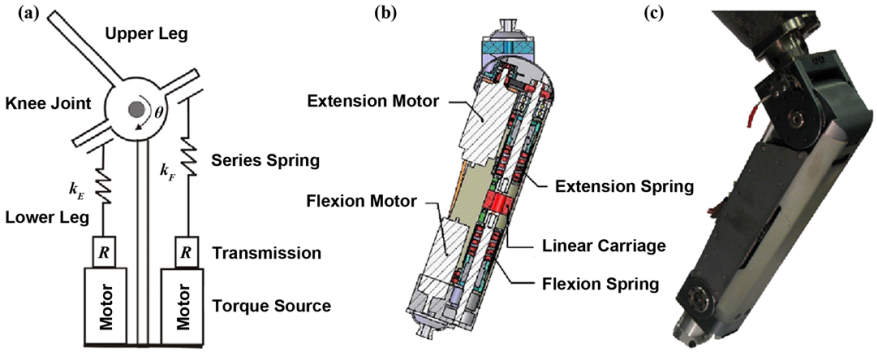

Figure 4.2: AAAKP design. **(a)** Simplified of the agonist-antagonist mechanical architecture. **(b)** Mechanical CAD design. **(c)** Photography of the knee prosthesis prototype.

4.2 AAKP Testing Methodology

The actual power knee prosthesis prototype will be used to validate the approach developed in this thesis. However, due to the architecture of the motors encoders, the electronic board embedded in the prototype and the corresponding controller, it is not straightforward to implement numerical integration in the AAAKP controller. Indeed, the current low-level controller of the device is based on a finite-state machine and each state has only a very limited number of operations allowed to be handled in (four floating-point multiplications seemed to be already beyond this limit) as well as a very limited time to stay in (less than $10ms$). Indeed, when the same state is required for the next step by the higher level control, the encoder exits and re-enters the same state again. Thus, the bottleneck limitation of this system is the limited number of operations allowed in each time step. Because of these limitations the implementation of a set of differential equations cannot be integrated within the device itself.

Moreover, the current AAAKP controller does not handle multi-threading (performing several operations or tasks at the same time). That would have allowed to achieve all the computations required for the generation of the desired

trajectory in an ad hoc parallel code execution while executing the position control in the finite state machine. Also, the possibility of performing all the required computations in a completely external software such as Matlab and streaming the output data in the controller was considered but such an implementation required way more time and expertise than available within the scope of this project.

Nevertheless, it is still of great interest to get a grasp of the challenges inherent to the hardware. It is also interesting to observe how the AAAKP tracks a desired trajectory when controlled in position, given a limited source of current for the DC motors i.e. a limited amount of torque available at the prosthetic knee joint. For these reasons and given the limitation aforementioned, the following compromise was implemented: A mathematical simulation is run on Matlab and the knee trajectory output generated by the playback pool of oscillator is extracted in a csv file. Then an array of two cycles is generated by interpolation (the integration frequency used on Matlab is $100Hz$ and the AAAKP controller runs at $400Hz$). The values in the array are then transformed from (rad) to the corresponding *number of motor clicks*, where 12566.93 clicks correspond to a full motor revolution.

The position controller computes the amount of input current required for each DC motor in order to track the desired trajectory hence playing back - offline - the output of the system presented in this study.

4.2.1 Position Controller

The AAAKP encoders and low level controller are not designed to achieve position control.
One rotation of the pulley corresponds to one rotation of the knee. The circumference of pulley is $15.96cm$. That means that 1 knee rotation equals $15.96cm$ of carriage linear travel, so the linear to rotational coefficient is:

$$15.96\frac{\text{cm of carriage linear travel}}{rotation_{knee}}$$

The linear encoder clicks/distance relation is:

$$2000\frac{\text{linear encoder clicks}}{in}\cdot\frac{1in}{2.54cm}=787.4\frac{\text{linear encoder clicks}}{cm}$$

Hence, the relation *linear encoder clicks* to *knee rotation* is:

$$787.4\frac{\text{linear encoder clicks}}{cm}\cdot 15.96\frac{\text{cm of carriage linear travel}}{rotation_{knee}}=12566.93\frac{\text{linear encoder clicks}}{rotation_{knee}}$$

Now regarding the DC rotational motors (M): 2 rotations of the motor corresponds to one rotation of the ballscrew (BS) that connects to the pulley. It also has a characteristic of 2000 motor clicks per motor rotation and 1 rotation of the ballscrew corresponds to 0.3cm of carriage linear travel:

$$\frac{2000clicks_M}{rotation_M}\cdot\frac{2rotation_M}{rotation_{BS}}\cdot\frac{1rotation_{BS}}{0.3cm\text{of linear travel}}\cdot\frac{15.96cm}{rotation_{knee}}=\frac{212800clicks_M}{rotation_{knee}}$$

Finally that gives the following motor clicks to knee flexion relation:

$$\frac{212800clicks_M}{rotation_{knee}}\cdot\frac{360deg}{1rotation_{knee}}=\frac{591clicks_M}{deg_{flexion}}$$

Which is the same for both the flexion and extension motor. When the target position requires a flexion the flexion motor pushes on the carriage while the extensor one tracks it on the other side and vice versa.

4.3 Results

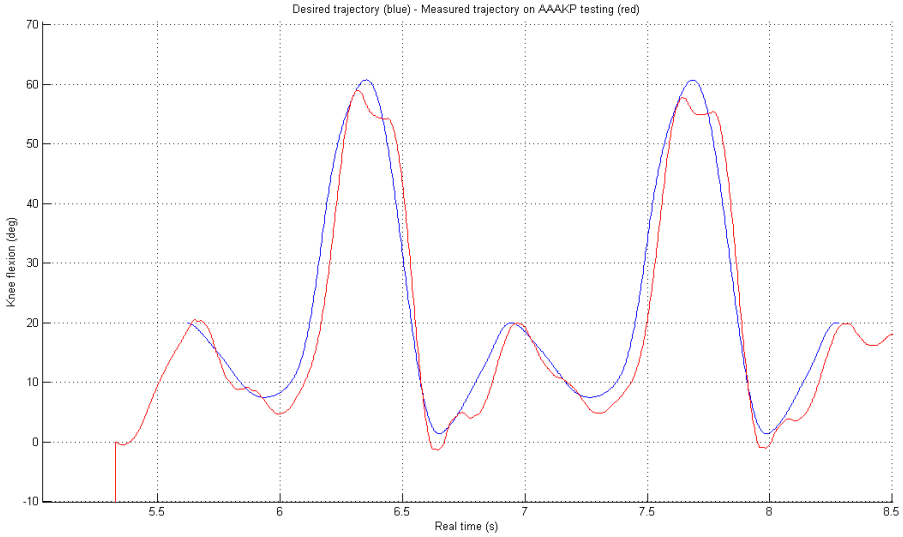

Figure 4.3: Trajectory playback on the AAAKP. In blue is the desired trajectory from the playback oscillators system. The red curve is the measured trajectory on the AAAKP. y-axis is the knee flexion (deg) - x-axis is real time (s).

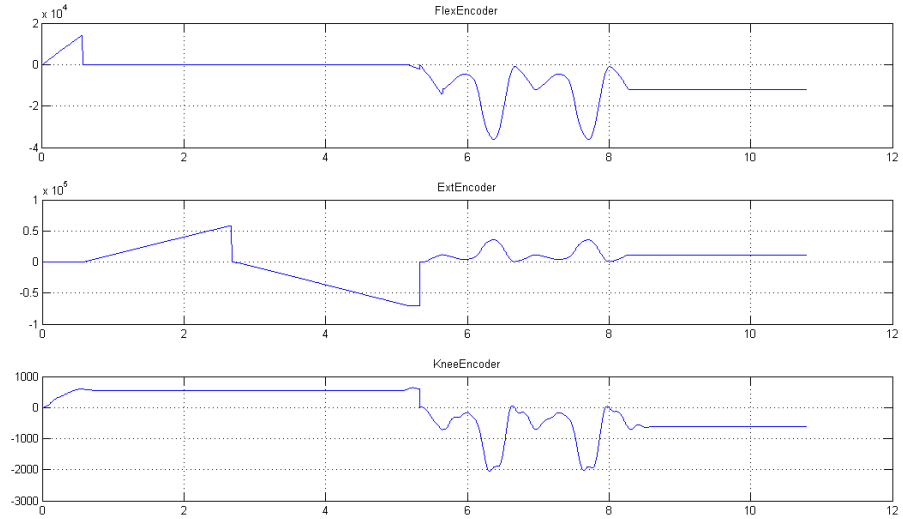

Figure 4.4: Contribution of the two DC motors: flexor and extensor resulting in the overall knee flexion angle given by the knee encoder. y-axis are motor positions (clicks) - x-axis is real time (s).

Chapter 5

General Discussion and Conclusion

In this conclusion chapter, we first briefly recall the aim of this study and summarize the main steps of the work presented in this document. Then we discuss the results, raise some of the limitations of the proposed strategy and mention the major contributions. Finally we discuss the different research perspectives raised by this work , both for the Webots model simulations and for control strategies in a wider sense.

5.1 Summary

5.1.1 System overview

In this study we intended to investigate the very challenging problem of lower limb robotic prosthesis control using central pattern generators. The CPG-based control architecture presented in this research is mainly made of two elements: The first element is an adaptive frequency oscillator (AFOs) that intends to decode the intention of the amputee by synchronizing to the acceleration signal from the hip. By providing this sensory feedback, this element constitutes the interface between the subject motion and the joint trajectory generator, which is the second system. This element receives from the first AFO the information of gait frequency and phase and uses it to trigger the online generation of trajectories for a prosthetic ankle, or knee, or both.

5.1.2 Research process and corresponding results

Adaptive CPG design As a first step in this investigation we implement a CPG model capable of learning and playing back a periodic signal. The system architecture is widely inspired by previous work done within the Biorobotics Laboratory, EPFL [1]. It consists of a set of coupled AFOs within a negative feedback loop. We run a simulation with a four sines signal as input to be learned and played back which successful results allow the validation of the implementation. Note that the same kind of dynamical system was recently used with humans in the loop to provide movement assistance using an elbow exoskeleton [23, 24].

Number of oscillators required Then we assess the number of oscillators allowing the playback signal to be close enough to the original signal. We find that five is a good number of oscillator: less makes the generated signal not accurate in term of fidelity to the anthropometric trajectory. Also we find that having more does not significantly improve the fidelity to justify the extra computational cost.

Learning of anthropometric joint trajectories Once the number of oscillators required is assessed we input to the adaptive CPG the anthropometric patterns of the knee and ankle at slow normal and fast walking. We test the CPG playback for each speed and joint and find that the reproduction is qualitatively satisfying, that is it is very close to the anthropometric teaching patterns. From the learning process we extract the amplitudes and phases of each frequency components for each speed of the knee and ankle trajectory.

Physics-based simulations Further we implemented the system described in section 5.1.1 in Webots, a physics-based robot simulation software. We use a bipedal model having one degree of freedom at each joint actuated by a rotational servo. First, we achieve a human-like gait by feeding anthropometric positions to the motors. Then we use the proposed system to actuate the knees and ankles of both legs, simulating prosthesis control. We achieve human like gait at each of the three walking speeds using accelerations from the hips as sensory feedback. Indeed, we find that the gait tracking using an AFO is satisfying as it allows

speed modulation. However, this requires a lot of hand tuning mostly for the gain of the frequency adaptation and the initial condition on the AFO frequency.

Powered knee testing In order to have an idea of how the system performs when implemented in an actual prosthetic knee, we extract the knee trajectory from a simulation of the system and play it on the Agonist Antagonist Active Knee prototype available in the Biomechatronics group, on a vertical test-bench setup. We found that it is able to track the desired position in a qualitatively satisfying way.

5.2 Discussion

The results observed for the CGP-based control of both knees and ankles are very encouraging as a human-like gait is achieved after less than 15 seconds of simulation. This is the time that is required for the system to stabilize. The reason is that the gait tracking relies on the motion of the legs which knees and ankles are controlled by the playback subsystem. The latter is in turn triggered by the the gait tracking AFO thus closing the loop of the control architecture. Moreover, when the hips abruptly switch from slow to fast walking, the system adapts in approximately 10 to 15s.

However, one should keep in mind some important limitations of the model:

The acceleration measured in Webots might be different from the one we would get in real world. It is likely that it will not be as periodic as in the simulations because in real world an amputee adapts his or her hip motion according to the response he gets from the prosthesis whereas in the simulations, the hips play a perfectly rhythmic and perfectly shaped pattern, regardless of what is happening below.

The chaotic behavior during the adaptation time is an intrinsic property of the proposed system. In simulations that does not affect much the movements of the hips but an amputee would completely lose the confidence in a device that

behaves in an unpredictable way for 10s before stabilizing. Actually, the amputee would likely fall down or stumble and stop walking before the system stabilizes.

The signal from the gait tracking AFO does not stop when the hips stop moving, potentially indicating the amputee's intention to stop walking thus keeping the knees and ankles moving. This is due to the system's intrinsic inertia, as mentioned earlier. However, it is likely that if the system was used to control only one ankle, for instance, this effect would be attenuated.

The rotational servos used in the Webots simulations provide satisfying tracking of the desired trajectories but in real world such a direct-drive control might be too stiff. A system using series elastic actuators as in the AAAKP would probably allow more flexibility in the control thus giving the amputee more confidence. A system that overreacts to perturbations could be dangerous for the patient.

5.2.1 Position control

This last point raises the interesting question of the relevance of a position control for knee and ankle prosthesis. In the case of the power ankle-foot developed in the Biomechatronics lab, it is commonly accepted among the community that position control is too difficult to achieve because of the very large amount of torque required at toe-off. Actually, most of the net power provided by the ankle is delivered at this precise time (right before toe-off) for the push-off. That makes it very challenging to time a position control in order to get the torque at this precise instant of the gait cycle. For that reason, impedance control[1] is largely preferred.

Moreover, it is known that human walking is a highly optimal process in which legs passive dynamics is largely used [36]. A simple position controller however tends to override this dynamic, not leverage it.

[1] in that context impedance control means that the motor is torque controlled depending on the position

For the knee, it is commonly accepted that, during stance, it should be locked or at least have a very constraint freedom of motion to support the amputee weight transfer. Then during swing the knee has to extend to prepare for the next heel strike. This extension has to be damped as a free knee would extend to fast because of the movement of the hips. This is precisely where a position control would be acceptable and useful. Indeed, it is of high importance that the knee angle be close to 4deg[1] at heel strike. More flexion will tend to make the amputee buckle and more extension will display an unnatural gait where the amputee reaches full knee extension too early.

In that sense, the results reported in this study are very encouraging for a control of knee damping as the proposed system provides a good estimation of the position the knee should follow giving the gait speed of the amputee.

5.3 Research Perspectives

5.3.1 Webots simulations

There are a some interesting questions to be raised and answered using the bipedal model on Webots. First it would be of great interest to test the ability of the control system to handle perturbations. For instance, one can implement ascending and descending slopes to observe how the system reacts and modulates parameters such as the gait tracking AFO gain. Also, investigating a coupling between each leg's gait tracking system could be of high relevance. This might shorten the stabilization time mentioned above but how should the coupling strength should be chosen? Should it be constant or vary with speed?

5.3.2 Hardware implementation

We mentioned that position control is likely to be too stiff to control a knee and ankle prosthesis at all gait phases. However, it would be of high interest to

[1] We believe there is no absolute correct value for the knee flexion at heelstrike. It depends on the gait style and speed, variable among trials and subjects. However, it must *feel* like it is the perfect angle for the amputee in order to ensure his confidence in the device.

implement the proposed control system on either a knee or a powered ankle-foot. That would allow to observe one important parameter: how does a human react and adapt with the system? Moreover, it would validate the approach using the acceleration signal to synchronize the gait tracking AFO with user's gait. Obviously, giving the position control, important security mechanisms should be implemented in order to avoid extreme behaviors caused by large errors between the actual position and the position desired by the control system. One possible mechanism is to chose the gain γ very small to allow more errors tolerance. We recall that γ determines the limit-cycle recovery speed.

5.3.3 Coupling with other control strategies

In the control strategy proposed here, the joint trajectories are predefined and embedded in the system. Though it integrates a sensory- feedback, such a design is still a widely feedforward one. We believe that a synergy with a more feedback oriented control system is an exciting perspective. For instance, in [37] a control based on neuromuscular reflex model is proposed. We believe that the position control of the system proposed in this system could be used in parallel with such a reflex based system. For instance, a weight function attributing more or less importance to one system with respect to the other (e.g based on gait speed) could make the controller more robust at all speeds. For instance the position control system could be useful for low speed gaits where few torque and reactivity is required whereas a more reflex-based control, being more responsive, would be more relevant for higher gait speeds. Moreover, the gait tracking subsystem can be helpful to modulate the reflex gains.

Appendix A: Results of CPG Anthropometric Patterns Learning

.1 Ankle Pattern

This section reports the results of the learning of the system in the same configuration as in subsection 2.1.4 for the ankle patterns at slow .1.1, normal .1.2 and fast .1.3 walking speed. The parameters specific to each pattern are the fundamental frequency, the corresponding amplitudes and phases relationships between the fundamental frequency and the harmonics and they are reported in tables 1, 2 and 3 for slow, normal and fast walking speed respectively.

.1.1 Slow walking speed

Oscillator#	1	2	3	4	5
Learned frequencies (rad/s)	7.95	15.90	23.86	31.81	39.77
Corresponding amplitudes (dimesionless)	0.10	0.11	0.06	0.03	0.02
Corresponding phases (dimensionless)	0	2.81	0.76	3.94	2.35

Table 1: Learning of the oscillators for *slow* walking speed - *ankle* trajectory.

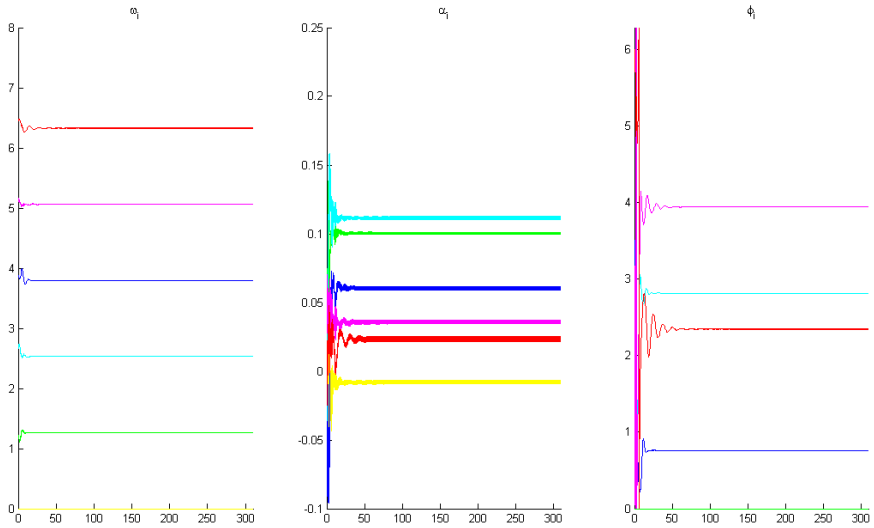

Figure 1: Convergence of the state variables ω_i, α_i and ϕ_i (plots left to right) during the learning of the *slow walking speed ankle trajectory*. x-axis is learning (i.e. simulation) time in (s). y-axis of the left plot is the frequency in (Hz). Other y-axis are dimensionless.

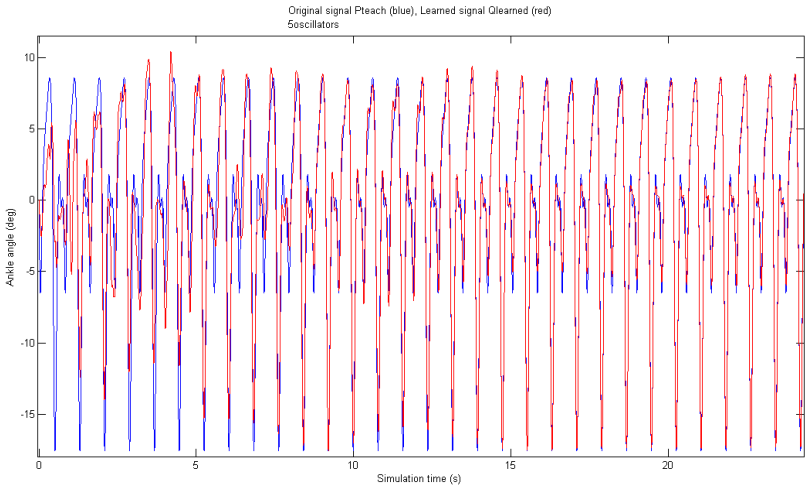

Figure 2: First seconds of the learning process for the *slow walking speed ankle pattern*. The blue line is the teaching signal i.e. P_{teach} and the red line is the learned signal i.e. $Q_{learned}$. x-axis are simulation time in (s). y-axis are ankle angle in (deg).

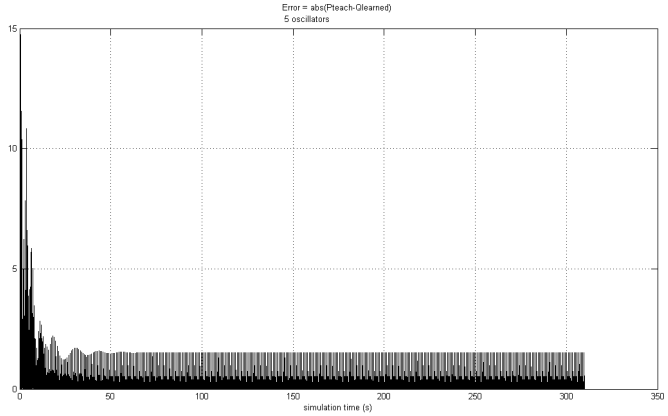

Figure 3: Evolution of the error between the teaching signal and the learned signal during the learning of the *slow walking speed ankle trajectory*. x-axis is learning (i.e. simulation) time in (s). y-axis is $abs(P_{teach} - Q_{learned})$

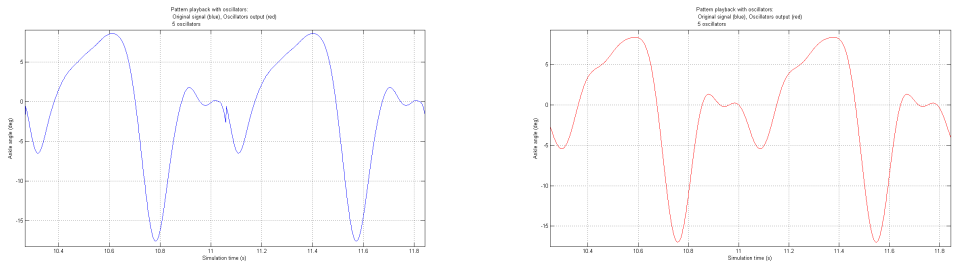

(a) Teaching signal

(b) Playback signal

Figure 4: Teaching signal 4(a) and oscillators playback 4(b) for *slow walking speed ankle trajectory*. x-axis are simulation time in (s). y-axis are ankle angle in (deg).

.1.2 Normal walking speed

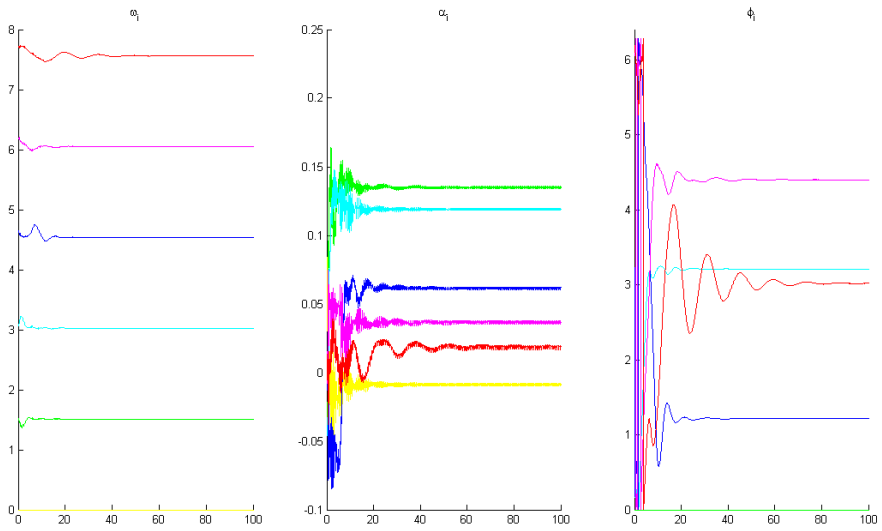

Figure 5: Convergence of the state variables ω_i, α_i and ϕ_i (plots left to right) during the learning of the *normal walking speed ankle trajectory*. x-axis is learning (i.e. simulation) time in (s). y-axis of the left plot is the frequency in (Hz). Other y-axis are dimensionless.

Oscillator#	1	2	3	4	5
Learned frequencies (rad/s)	9.50	19.01	28.52	38.02	47.53
Corresponding amplitudes (dimesionless)	0.13	0.12	0.06	0.04	0.01
Corresponding phases (dimensionless)	0	3.21	1.21	4.40	3.02

Table 2: Learning of the oscillators for *normal* walking speed - *ankle* trajectory.

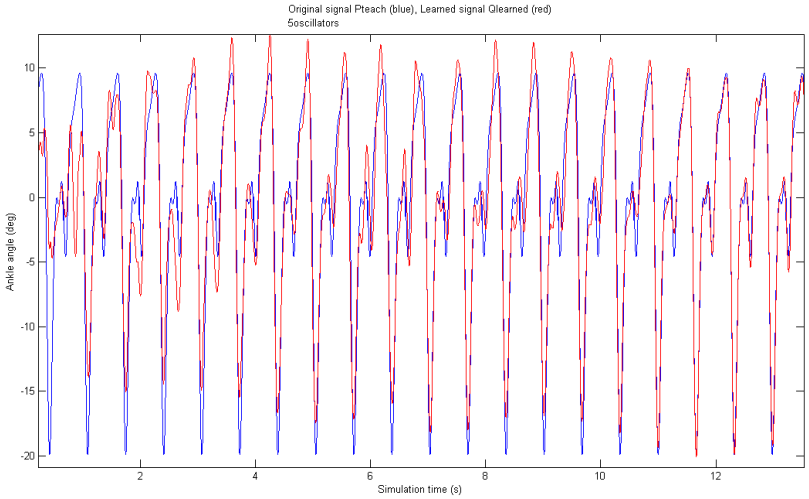

Figure 6: First seconds of the learning process for the *normal walking speed ankle pattern*. The blue line is the teaching signal i.e. P_{teach} and the red line is the learned signal i.e. $Q_{learned}$. x-axis are simulation time in (s). y-axis are ankle angle in (deg).

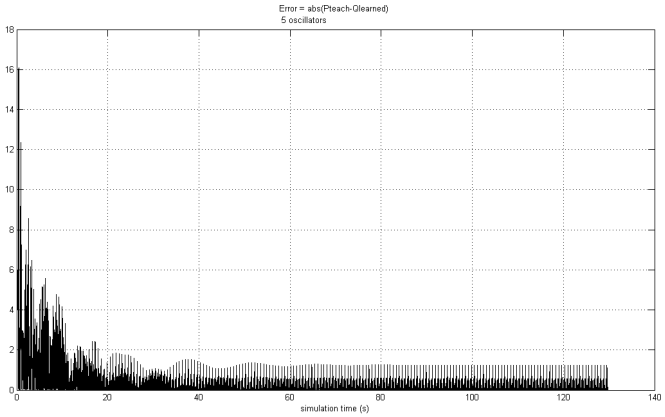

Figure 7: Evolution of the error between the teaching signal and the learned signal during the learning of the *normal walking speed ankle trajectory*. x-axis is learning (i.e. simulation) time in (s). y-axis is $abs(P_{teach} - Q_{learned})$

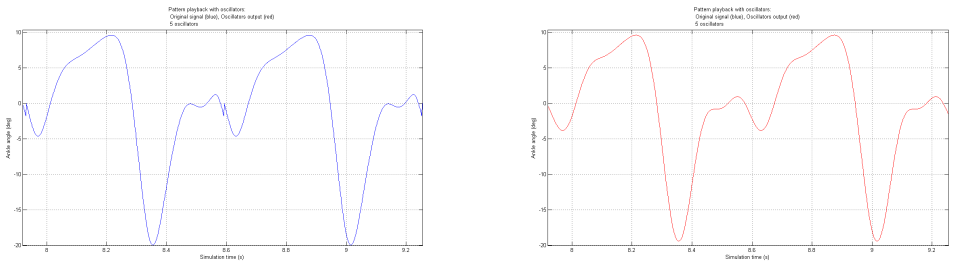

(a) Teaching signal

(b) Playback signal

Figure 8: Teaching signal 8(a) and oscillators playback 8(b) for *normal walking speed ankle trajectory*. x-axis are simulation time in (s). y-axis are ankle angle in (deg).

.1.3 Fast walking speed

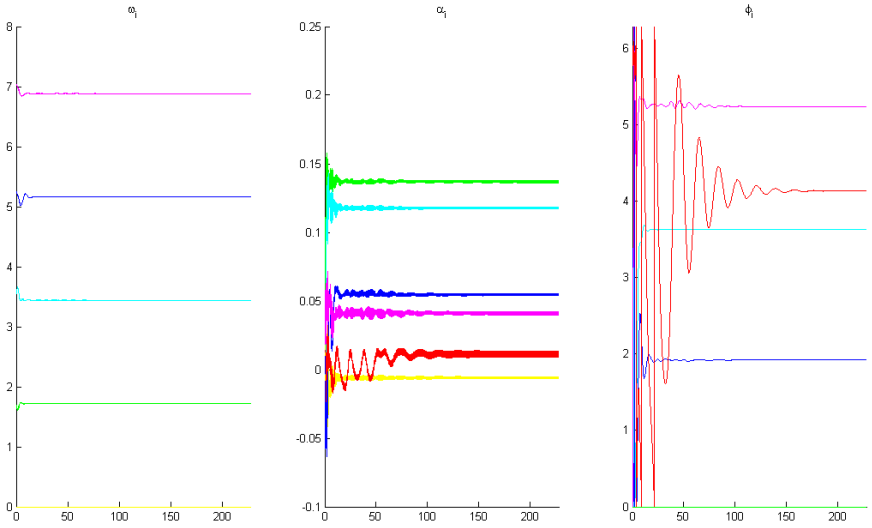

Figure 9: Convergence of the state variables ω_i, α_i and ϕ_i (plots left to right) during the learning of the *fast walking speed ankle trajectory*. x-axis is learning (i.e. simulation) time in (s). y-axis of the left plot is the frequency in (Hz). Other y-axis are dimensionless.

Oscillator#	1	2	3	4	5
Learned frequencies (rad/s)	10.81	21.63	32.44	43.26	54.07
Corresponding amplitudes (dimesionless)	0.14	0.12	0.05	0.04	0.01
Corresponding phases (dimensionless)	0	3.63	1.92	5.24	4.13

Table 3: Learning of the oscillators for *fast* walking speed - *ankle* trajectory.

.2 Knee Pattern

This section reports the results of the learning of the system in the same configuration as in subsection 2.1.4 for the three ankle patters i.e. slow, normal and fast walking speed. The parameters specific to each pattern are the fundamental frequency, the corresponding amplitudes and phases relationships between the fundamental frequency and the harmonics.

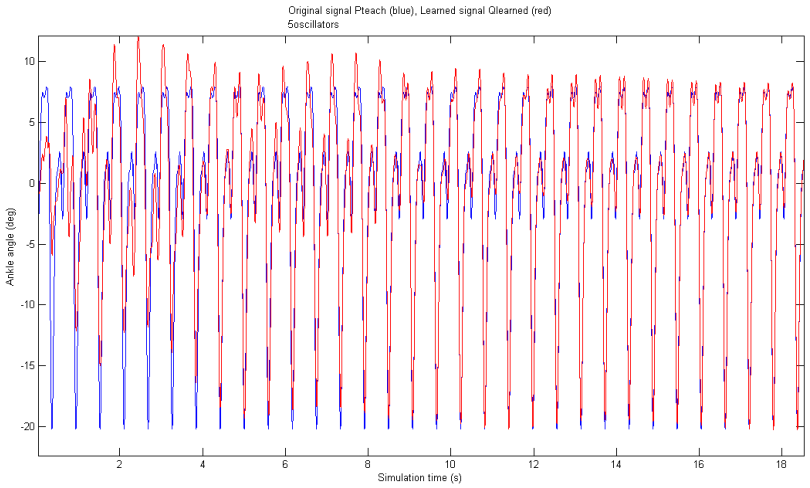

Figure 10: First seconds of the learning process for the *fast walking speed ankle pattern*. The blue line is the teaching signal i.e. P_{teach} and the red line is the learned signal i.e. $Q_{learned}$. x-axis are simulation time in (s). y-axis are ankle angle in (deg).

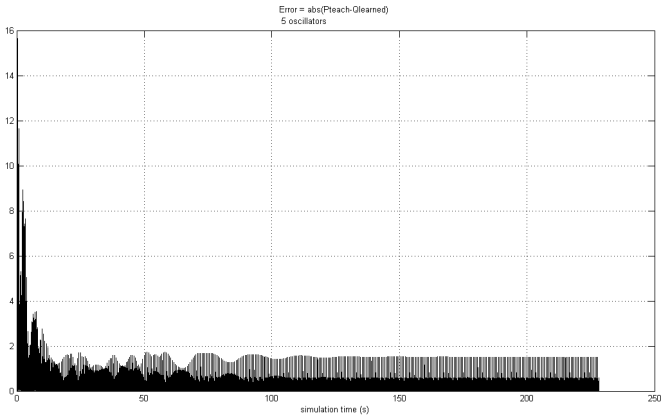

Figure 11: Evolution of the error between the teaching signal and the learned signal during the learning of the *fast walking speed ankle trajectory*. x-axis is learning (i.e. simulation) time in (s). y-axis is $abs(P_{teach} - Q_{learned})$

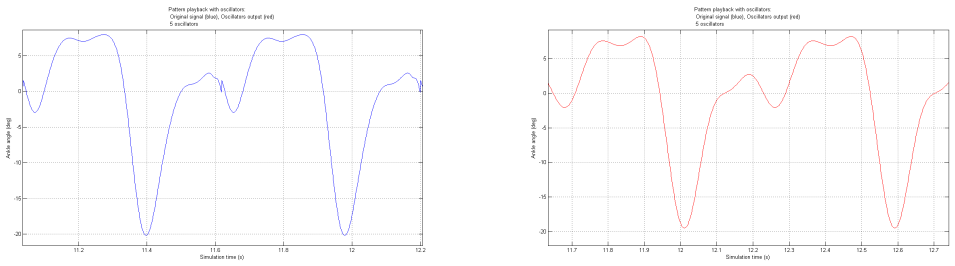

(a) Teaching signal

(b) Playback signal

Figure 12: Teaching signal 12(a) and oscillators playback 12(b) for *fast walking speed ankle trajectory*. x-axis are simulation time in (s). y-axis are ankle angle in (deg).

.2.1 Slow walking speed

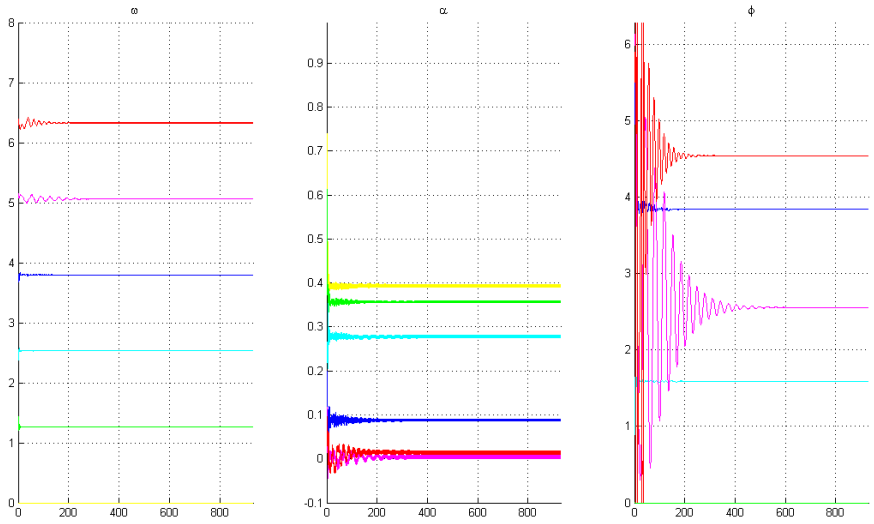

Figure 13: Convergence of the state variables ω_i, α_i and ϕ_i (plots left to right) during the learning of the *slow walking speed knee trajectory*. x-axis is learning (i.e. simulation) time in (s). y-axis of the left plot is the frequency in (Hz). Other y-axis are dimensionless.

Oscillator#	1	2	3	4	5
Learned frequencies (rad/s)	7.95	15.90	23.86	31.81	39.77
Corresponding amplitudes (dimesionless)	0.36	0.28	0.09	0.06	0.01
Corresponding phases (dimensionless)	0	1.59	3.84	2.55	4.54

Table 4: Learning of the oscillators for *slow* walking speed - *knee* trajectory.

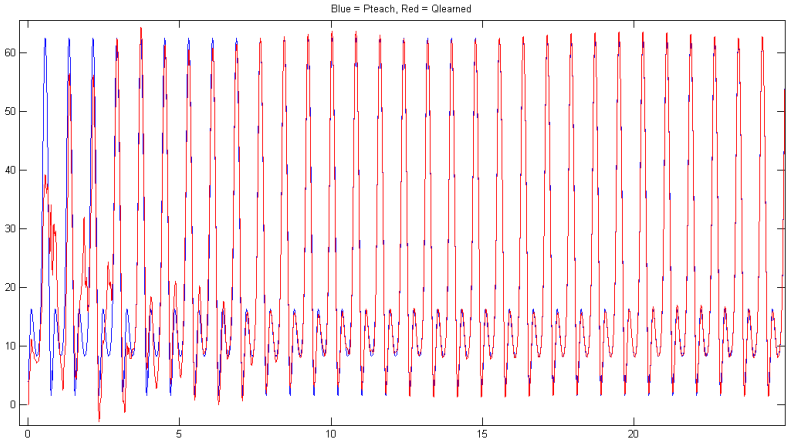

Figure 14: First seconds of the learning process for the *slow walking speed knee pattern*. The blue line is the teaching signal i.e. P_{teach} and the red line is the learned signal i.e. $Q_{learned}$. x-axis are simulation time in (s). y-axis are knee angle in (deg).

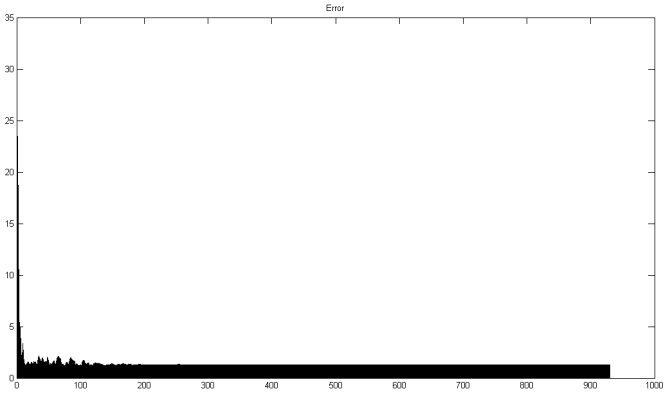

Figure 15: Evolution of the error between the teaching signal and the learned signal during the learning of the *slow walking speed knee trajectory*. x-axis is learning (i.e. simulation) time in (s). y-axis is $abs(P_{teach} - Q_{learned})$

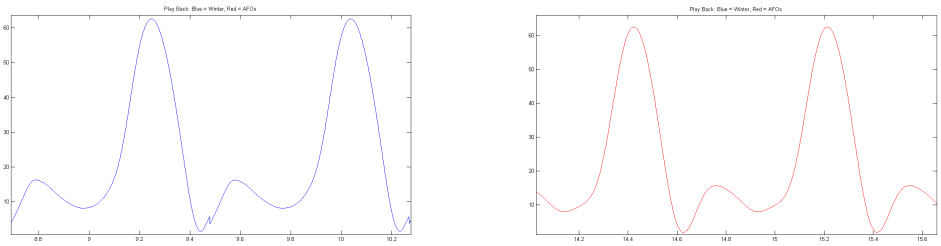

(a) Teaching signal (b) Playback signal

Figure 16: Teaching signal 16(a) and oscillators playback 16(b) for *slow walking speed knee trajectory*. x-axis are simulation time in (s). y-axis are knee angle in (deg).

.2.2 Normal walking speed

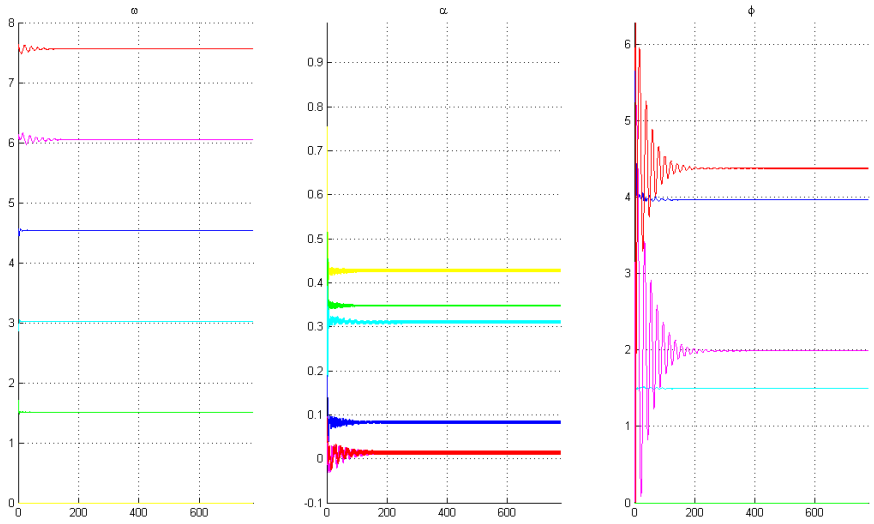

Figure 17: Convergence of the state variables ω_i, α_i and ϕ_i (plots left to right) during the learning of the *normal walking speed knee trajectory*. x-axis is learning (i.e. simulation) time in (s). y-axis of the left plot is the frequency in (Hz). Other y-axis are dimensionless.

Oscillator#	1	2	3	4	5
Learned frequencies (rad/s)	9.50	19.01	28.52	38.02	47.53
Corresponding amplitudes (dimesionless)	0.35	0.31	0.08	0.01	0.01
Corresponding phases (dimensionless)	0	1.49	3.96	1.99	4.37

Table 5: Learning of the oscillators for *normal* walking speed - *knee* trajectory.

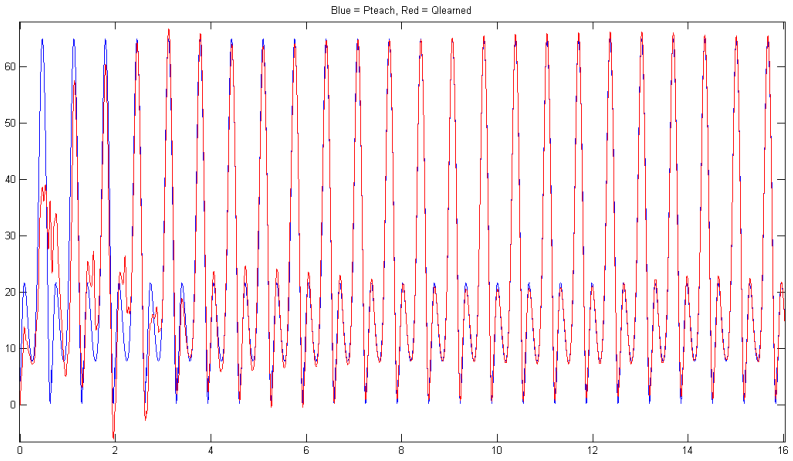

Figure 18: First seconds of the learning process for the *normal walking speed knee pattern*. The blue line is the teaching signal i.e. P_{teach} and the red line is the learned signal i.e. $Q_{learned}$. x-axis are simulation time in (s). y-axis are knee angle in (deg).

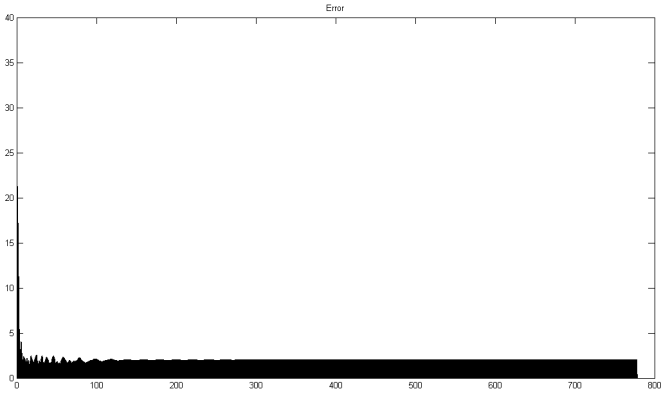

Figure 19: Evolution of the error between the teaching signal and the learned signal during the learning of the *normal walking speed knee trajectory*. x-axis is learning (i.e. simulation) time in (s). y-axis is $abs(P_{teach} - Q_{learned})$

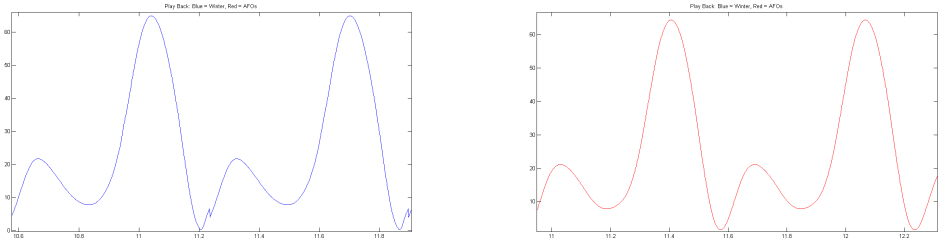

(a) Teaching signal

(b) Playback signal

Figure 20: Teaching signal 20(a) and oscillators playback 20(b) for *normal walking speed knee trajectory*. x-axis are simulation time in (s). y-axis are knee angle in (deg).

.2.3 Fast walking speed

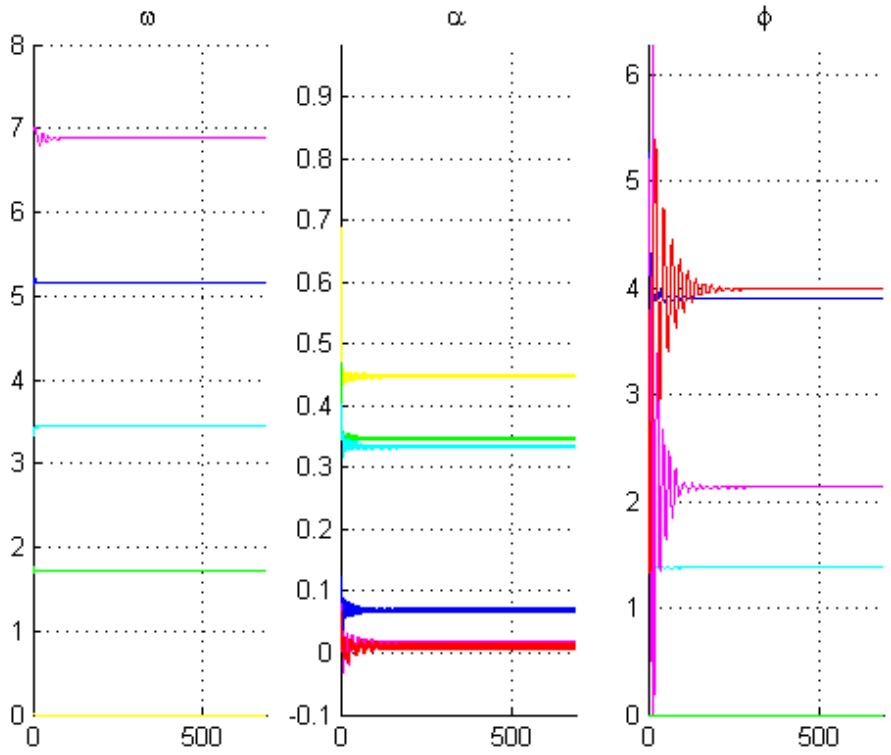

Figure 21: Convergence of the state variables ω_i, α_i and ϕ_i (plots left to right) during the learning of the *fast walking speed knee trajectory*. x-axis is learning (i.e. simulation) time in (s). y-axis of the left plot is the frequency in (Hz). Other y-axis are dimensionless.

Oscillator#	1	2	3	4	5
Learned frequencies (rad/s)	10.81	21.63	32.44	43.26	54.07
Corresponding amplitudes (dimesionless)	0.35	0.33	0.07	0.02	0.01
Corresponding phases (dimensionless)	0	1.38	3.91	2.13	3.99

Table 6: Learning of the oscillators for *fast* walking speed - *knee* trajectory.

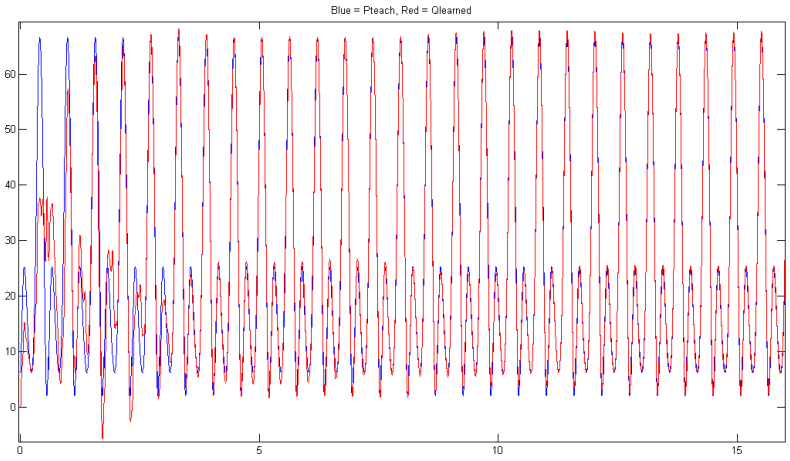

Figure 22: First seconds of the learning process for the *fast walking speed knee pattern*. The blue line is the teaching signal i.e. P_{teach} and the red line is the learned signal i.e. $Q_{learned}$. x-axis are simulation time in (s). y-axis are knee angle in (deg).

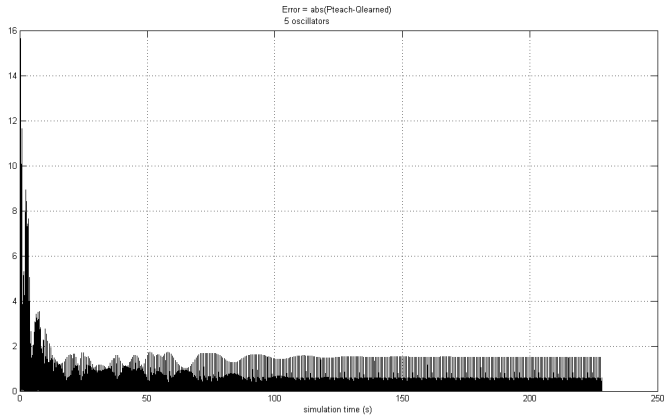

Figure 23: Evolution of the error between the teaching signal and the learned signal during the learning of the *fast walking speed knee trajectory*. x-axis is learning (i.e. simulation) time in (s). y-axis is $abs(P_{teach} - Q_{learned})$

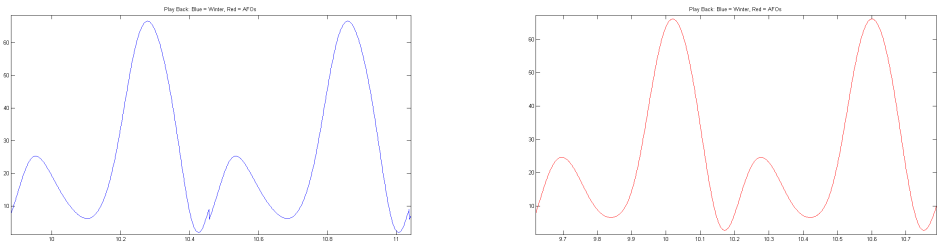

(a) Teaching signal

(b) Playback signal

Figure 24: Teaching signal 24(a) and oscillators playback 24(b) for *fast walking speed knee trajectory*. x-axis are simulation time in (s). y-axis are knee angle in (deg).

References

[1] L. Righetti and A.J. Ijspeert. Programmable central pattern generators: an application to biped locomotion control. In *Proceedings of the 2006 IEEE international conference on robotics and automation*, pages 1585–1590. Citeseer, 2006. 7, 3, 13, 15, 16, 17, 49

[2] DA Winter. The Biomechanics and Motor Control of Human Gait: Normal. *Elderly and Pathalogical, second ed., Waterloo Biomechanics, Waterloo, Ont*, 1991. 7, 1, 17, 19, 20, 32

[3] E.C. Martinez-Villalpando and H. Herr. Agonist-antagonist active knee prosthesis: a preliminary study in level-ground walking. *Journal of rehabilitation research and development*, 46(3):361, 2009. 9, 2, 8, 42, 43

[4] Kate Wong. Ancient egyptian prosthetic surgery. *Scientific American*, 2003. 1

[5] P. De Vita, M. Torry, K.L. Glover, and D.L. Speroni. A functional knee brace alters joint torque and power patterns during walking and running. *Journal of biomechanics*, 29(5):583–588, 1996. 1

[6] B.I. Prilutsky, L.N. Petrova, and L.M. Raitsin. Comparison of mechanical energy expenditure of joint moments and muscle forces during human locomotion. *Journal of biomechanics*, 29(4):405–415, 1996. 1

[7] M.W. Whittle. Clinical gait analysis: A review. *Human Movement Science*, 15(3):369–387, 1996. 2, 4

[8] J.L. Johansson, D.M. Sherrill, P.O. Riley, P. Bonato, and H. Herr. A clinical comparison of variable-damping and mechanically passive prosthetic knee devices. *American Journal of Physical Medicine & Rehabilitation*, 84(8): 563, 2005. 2, 4

[9] R.L. Waters and S. Mulroy. The energy expenditure of normal and pathologic gait. *Gait & Posture*, 9(3):207–231, 1999. 2

[10] RF Goldman and PF Iampietro. Energy cost of load carriage. *Journal of Applied Physiology*, 17(4):675, 1962. 2

[11] A.J. Ijspeert. Central pattern generators for locomotion control in animals and robots: a review. *Neural Networks*, 21(4):642–653, 2008. 2

[12] J. Duysens and H. Van de Crommert. Neural control of locomotion. Part 1: The central pattern generator from cats to humans. *Gait Posture*, 7:131–141, 1998. 2

[13] G.N. Orlovsky, TG Deliagina, and S. Grillner. *Neuronal control of locomotion: from mollusc to man*. Oxford University Press, USA, 1999. 2

[14] A.J. Ijspeert, A. Crespi, D. Ryczko, and J.M. Cabelguen. From swimming to walking with a salamander robot driven by a spinal cord model. *Science*, 315(5817):1416, 2007. 2

[15] JJ Collins and I. Stewart. Hexapodal gaits and coupled nonlinear oscillator models. *Biological Cybernetics*, 68(4):287–298, 1993. 2

[16] K. Seo, S.J. Chung, and J.J.E. Slotine. CPG-based control of a turtle-like underwater vehicle. *Autonomous Robots*, 28(3):247–269, 2010. 2

[17] G. Endo, J. Morimoto, J. Nakanishi, and G. Cheng. An empirical exploration of a neural oscillator for biped locomotion control. In *2004 IEEE International Conference on Robotics and Automation, 2004. Proceedings. ICRA'04*, volume 3. 2

[18] G. Taga. A model of the neuro-musculo-skeletal system for human locomotion. *Biological Cybernetics*, 73(2):97–111, 1995.

[19] D. Zhang and K. Zhu. Model and control of the locomotion of a biomimic musculoskeletal biped. *Artificial Life and Robotics*, 10(2):91–95, 2006.

[20] G.L. Liu, M.K. Habib, K. Watanabe, and K. Izumi. Central pattern generators based on Matsuoka oscillators for the locomotion of biped robots. *Artificial Life and Robotics*, 12(1):264–269, 2008.

[21] Q.D. Wu, C.J. Liu, J.Q. Zhang, and Q.J. Chen. Survey of locomotion control of legged robots inspired by biological concept. *Science in China Series F: Information Sciences*, 52(10):1715–1729, 2009.

[22] J.K. Ryu, N.Y. Chong, B.J. You, and H. Christensen. Adaptive CPG based coordinated control of healthy and robotic lower limb movements. In *The 18th IEEE International Symposium on Robot and Human Interactive Communication, 2009. RO-MAN 2009*, pages 122–127, 2009. 2

[23] T. Lenzi J. van den Kieboom M. C. Carrozza R. Ronsse, N. Vitiello and A. J. Ijspeert. Human-robot synchrony: Flexible assistance using adaptive oscillators. *submitted*. 3, 49

[24] T. Lenzi J. van den Kieboom M. C. Carrozza R. Ronsse, N. Vitiello and A. J. Ijspeert. Adaptive oscillators with human-in-the-loop: Proof of concept for assistance and rehabilitation. In *3rd IEEE RAS & EMBS International Conference on Biomedical Robotics and Biomechatronics (accepted)*, 2010. 3, 49

[25] B.J. Hafner, L.L. Willingham, N.C. Buell, K.J. Allyn, and D.G. Smith. Evaluation of function, performance, and preference as transfemoral amputees transition from mechanical to microprocessor control of the prosthetic knee. *Archives of physical medicine and rehabilitation*, 88(2):207–217, 2007. 8

[26] F. Sup, A. Bohara, and M. Goldfarb. Design and Control of a Powered Knee and Ankle Prosthesis. In *2007 IEEE International Conference on Robotics and Automation*, pages 4134–4139, 2007. 8

[27] F. Sup, A. Bohara, and M. Goldfarb. Design and control of a powered transfemoral prosthesis. *The International journal of robotics research*, 27 (2):263, 2008. 9

[28] S. Au, M. Berniker, and H. Herr. Powered ankle-foot prosthesis to assist level-ground and stair-descent gaits. *Neural Networks*, 21(4):654–666, 2008. 9, 10

[29] J. Hitt, T. Sugar, M. Holgate, R. Bellman, and K. Hollander. Robotic transtibial prosthesis with biomechanical energy regeneration. *Industrial Robot: An International Journal*, 36(5):441–447, 2009. 10

[30] S.H. Collins and A.D. Kuo. Recycling Energy to Restore Impaired Ankle Function during Human Walking. 2010. 10

[31] L. Righetti, J. Buchli, and A.J. Ijspeert. Dynamic hebbian learning in adaptive frequency oscillators. *Physica D: Nonlinear Phenomena*, 216(2):269–281, 2006. 11, 12, 13

[32] S.H. Strogatz. *Nonlinear dynamics and chaos: With applications to physics, biology, chemistry, and engineering*. Westview Pr, 2000. 12

[33] A. Pikovsky, M. Rosenblum, J. Kurths, and R.C. Hilborn. Synchronization: A universal concept in nonlinear science. *American Journal of Physics*, 70: 655, 2002. 13

[34] J.M. Hausdorff, CK Peng, Z. Ladin, J.Y. Wei, and AL Goldberger. Is walking a random walk? Evidence for long-range correlations in stride interval of human gait. *Journal of Applied Physiology*, 78(1):349, 1995. 20

[35] K. Endo, D. Paluska, and H. Herr. A quasi-passive model of human leg function in level-ground walking. In *2006 IEEE/RSJ International Conference on Intelligent Robots and Systems*, pages 4935–4939, 2006. 42

[36] T. McGeer. Passive dynamic walking. *The International Journal of Robotics Research*, 9(2):62, 1990. 51

[37] M. Eilenberg, H. Geyer, and H. Herr. Control of a Powered Ankle-Foot Prosthesis Based on a Neuromuscular Model. *IEEE transactions on neural systems and rehabilitation engineering: a publication of the IEEE Engineering in Medicine and Biology Society*, 2010. 53